catalysts

MDPI

Review

Application of TiO_2-Based Photocatalysts to Antibiotics Degradation: Cases of Sulfamethoxazole, Trimethoprim and Ciprofloxacin

Anastasiya Kutuzova [1,2,*], Tetiana Dontsova [2] and Witold Kwapinski [3]

[1] Leibniz Institute for Catalysis (LIKAT), Albert-Einstein-Straße 29a, 18059 Rostock, Germany
[2] Department of Technology of Inorganic Substances, Water Treatment and General Chemical Technology, Igor Sikorsky Kyiv Polytechnic Institute, Prosp. Peremohy 37, 03056 Kyiv, Ukraine; dontsova@xtf.kpi.ua
[3] Department of Chemical Sciences, Faculty of Science and Engineering, Bernal Institute, University of Limerick, Limerick V94 T9PX, Ireland; witold.kwapinski@ul.ie
* Correspondence: Anastasiya.Kutuzova@catalysis.de; Tel.: +49381-1281-335

Abstract: The extensive application of antibiotics in human and veterinary medicine has led to their widespread occurrence in a natural aquatic environment. Global health crisis is associated with the fast development of antimicrobial resistance, as more and more infectious diseases cannot be treated more than once. Sulfamethoxazole, trimethoprim and ciprofloxacin are the most commonly detected antibiotics in water systems worldwide. The persistent and toxic nature of these antibiotics makes their elimination by conventional treatment methods at wastewater treatment plants almost impossible. The application of advanced oxidation processes and heterogeneous photocatalysis over TiO_2-based materials is a promising solution. This highly efficient technology has the potential to be sustainable, cost-efficient and energy-efficient. A comprehensive review on the application of various TiO_2-based photocatalysts for the degradation of sulfamethoxazole, trimethoprim and ciprofloxacin is focused on highlighting their photocatalytic performance under various reaction conditions (different amounts of pollutant and photocatalyst, pH, light source, reaction media, presence of inorganic ions, natural organic matter, oxidants). Mineralization efficiency and ecotoxicity of final products have been also considered. Further research needs have been presented based on the literature findings. Among them, design and development of highly efficient under sunlight, stable, recyclable and cost-effective TiO_2-based materials; usage of real wastewaters for photocatalytic tests; and compulsory assessment of products ecotoxicity are the most important research tasks in order to meet requirements for industrial application.

Keywords: TiO_2 photocatalysis; sulfamethoxazole; trimethoprim; ciprofloxacin; visible light; advanced oxidation processes; antibiotics; emerging pollutants

Citation: Kutuzova, A.; Dontsova, T.; Kwapinski, W. Application of TiO_2-Based Photocatalysts to Antibiotics Degradation: Cases of Sulfamethoxazole, Trimethoprim and Ciprofloxacin. *Catalysts* **2021**, *11*, 728. https://doi.org/10.3390/catal11060728

Academic Editor: Fotis Katsaros

Received: 14 May 2021
Accepted: 11 June 2021
Published: 12 June 2021

1. Introduction

Pharmaceuticals (analgesics and anti-inflammatories, antibiotics, anticonvulsants, β-blockers, endocrine active pharmaceuticals, lipid regulators, psychiatric drugs [1]) have become an essential part of our life, benefiting society's health and wellbeing. Improved life expectancy, the better prevention of diseases and significantly reduced mortality could not be imagined without appropriate medication [2]. The consumption of pharmaceuticals continues to rise because of the ongoing demographical changes: growing world population, population density and aging societies (especially in developed countries) [1,3]. A growing population also means that more food is needed, leading to the increase in number and density of livestock, especially in intensive farming [1]. As a result, the demand for pharmaceuticals used for veterinary purposes also rises. Besides, the continuous progress of medical science, improvements in research and development, high health-care investments and the availability of the global market contribute to the development of more and more new drugs and their wider availability [2,3].

However, a huge environmental concern arises when pharmaceutical substances enter natural aquatic ecosystems [1,2,4,5]. Approximately 2000 pharmaceutically active compounds are administered globally in prescription and non-prescription medicines, as well as veterinary drugs [1,6]. These active pharmaceutical ingredients (APIs) are complex molecules that belong to micropollutants, as they are found in the range of ng/L–µg/L in water bodies [7]. APIs are being found worldwide (Figure 1) in surface water, groundwater, seawater, drinking water, sediment, soil, manure and biota [3,6,8,9]. Such a widespread occurrence of pharmaceuticals is a result of their high consumption and increased production [1].

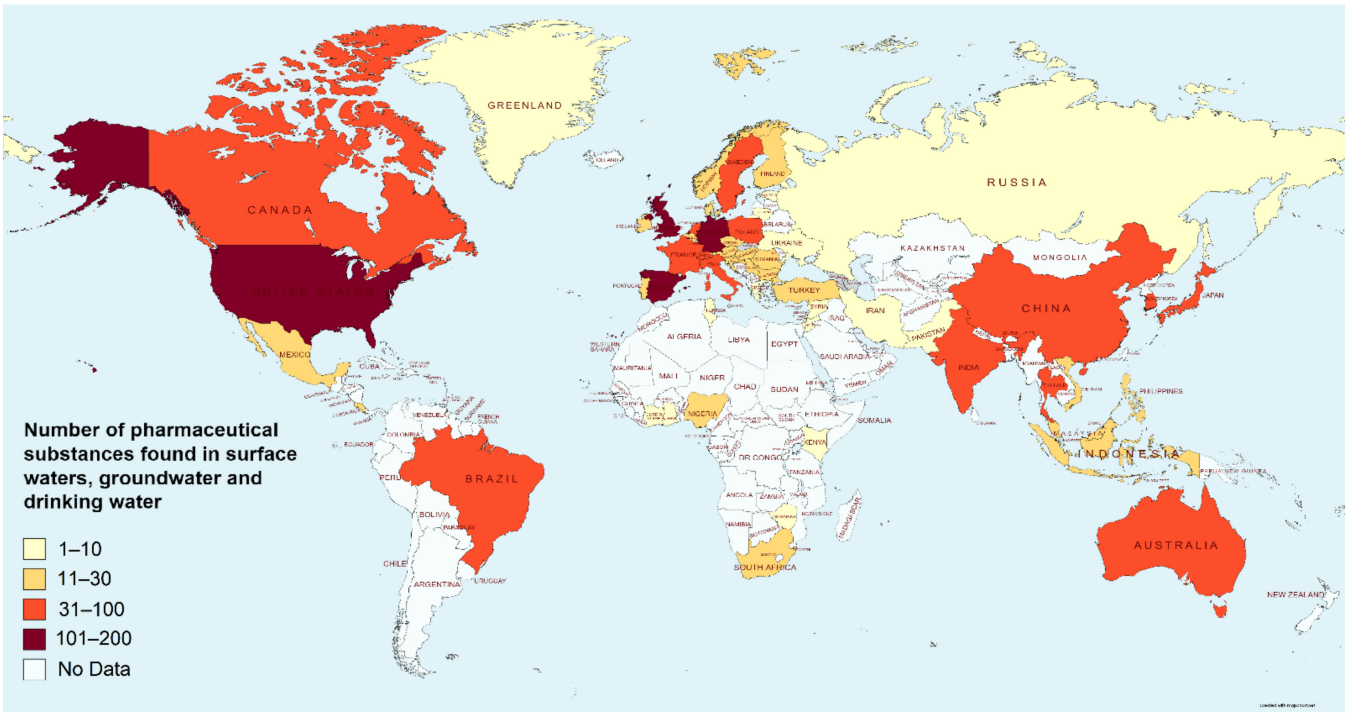

Figure 1. Global occurrence of pharmaceuticals.

1.1. Antibiotics Occurrence in Aqueous Environment

Among all the pharmaceuticals, antibiotics pose one of the most significant concerns. They are widely used to treat human infectious diseases, as well as for the treatment and prevention of infections in animals, apart from promoting their growth [10,11]. Approximately 100,000 tons [12,13] of antibiotics are manufactured annually in the world, and 50–60% of this amount is spent on veterinary purposes [8,13,14].

Antibiotics are chemotherapeutic agents that kill or inhibit the metabolic activity of various microorganisms, such as bacteria, fungi, viruses, microalgae or protozoa [9,11,15,16]. They can be natural, synthetic or semi-synthetic compounds, which show antibacterial, antiparasitic or antifungal activities [11,16]. There are different groups of antibiotics, depending on their mechanism of action or chemical structure. They are, for example, β-lactams (amoxicillin, cefalexin), aminoglycosides (kanamycin, neomycin, streptomycin), diaminopyrimidines (trimethoprim), glycopeptides (teicoplanin, vancomycin), macrolides (azithromycin, erythromycin, tylosin), quinolones (enrofloxacin, ciprofloxacin, levofloxacin, norfloxacin, ofloxacin), sulfonamides (sulfamethoxazole, sulfathiazole, sulfamethazine), tetracyclines (tetracycline, oxytetracycline) and others [4,10,11,14]. According to the assessment of antibiotic consumption in 76 countries, global consumption grew to 42.3 billion defined daily doses (DDDs) between 2000 and 2015, which is a 39% increase [6,16] and is still growing. The reason for that is obviously growth of population and, therefore, increasing demand of the animal protein [16]. As a result, antibiotics are being found in natural

water bodies across the whole world [4,9,12]—concentrations of different antibiotics from various classes found in surface waters, in areas away from wastewater treatment plants (WWTPs) and industrial production sites, are depicted in Figure 2.

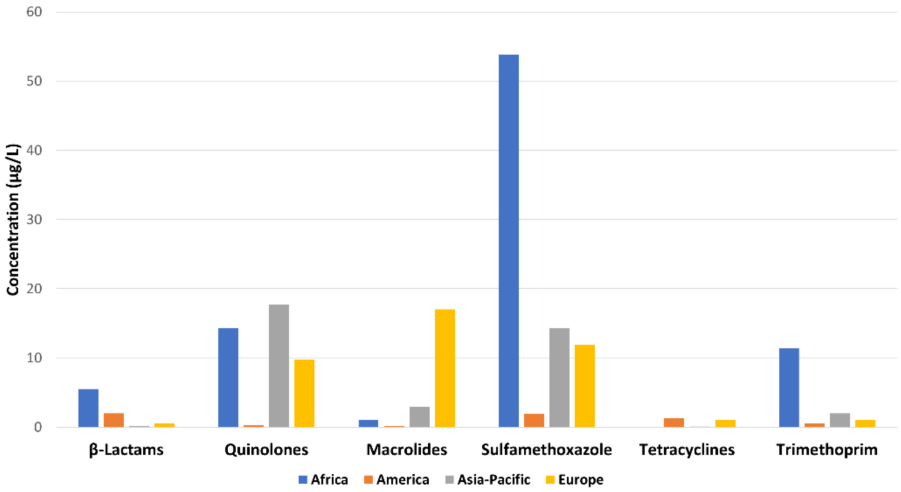

Figure 2. Antibiotics concentrations in surface waters across the world.

Although individual antibiotics are always detected at quite low concentrations, ranging from ng/L to µg/L [10,17], the simultaneous presence of several antibiotics even at low concentrations might result in their much stronger cumulative effect [14,16]. Properties of antibiotics clearly demonstrate why their presence in natural aquatic environment is highly undesirable: antibiotics are, first of all, persistent, so that they are non-degradable and are able to withstand natural decomposition [1,6,18]. Secondly, they are highly mobile, bioaccumulative and toxic [1,2,19]. Antibiotics are deliberately designed to affect living organisms and cause pharmacological response even at low doses. This means that aquatic organisms exposed to such pharmaceuticals may develop negative chronic effects, which affect their behavior, growth and reproduction [16].

1.2. Sulfamethoxazole, Trimethoprim and Ciprofloxacin as Antibiotics of Great Concern

Among the antibiotics, sulfamethoxazole (SMX), trimethoprim (TMP) and ciprofloxacin (CIP) are the most often detected substances [3,12,15] (Table 1, Scheme 1, their physico-chemical properties are presented in Table 2). These pharmaceuticals have been found at high concentrations in influents and effluents of wastewater treatment plants, surface waters (rivers and seas), groundwater, and drinking water, not only across Europe, but worldwide [15,20,21]. Apart from that, maximum concentrations of SMX, TMP and CIP detected in Africa were ~100 times, ~54 times and ~125 times, respectively, higher than those in Europe [22]. This happens because these antibiotics are widely used in human and veterinary medicine, have the largest numbers of manufacturers [22], are toxic and persistent in the aquatic environment [4,16].

Table 1. Concentrations of SMX, TMP and CIP detected in surface waters worldwide.

Antibiotic	Sulfamethoxazole	Trimethoprim	Ciprofloxacin
Number of countries where antibiotic was detected	47	29	20
Average concentration (µg/L)	0.095	0.037	18.99
Maximum concentration (µg/L)	53.8	13.6	6500

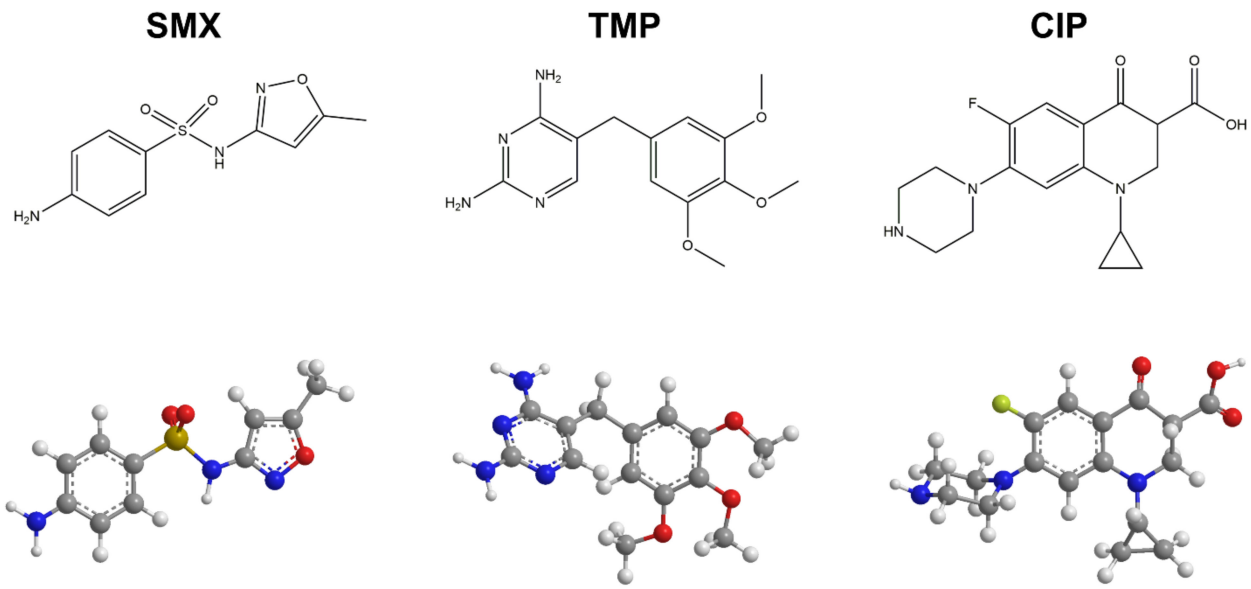

Scheme 1. Molecular structure of SMX, TMP and CIP and their 3D models.

Table 2. Physicochemical properties of SMX, TMP and CIP.

Antibiotic	Sulfamethoxazole	Trimethoprim	Ciprofloxacin
Class	Sulfonamides	Diaminopyrimidines	Fluoroquinolones
Molecular formula	$C_{10}H_{11}N_3O_3S$	$C_{14}H_{18}N_4O_3$	$C_{17}H_{18}FN_3O_3$
Molecular weight (g/mol)	253.28	290.32	331.34
pK_{a1}, pK_{a2}	1.7; 5.6 [23]	3.2; 6.7 [23]	5.9; 8.9 [24]
Solubility in water (mg/L) [8]	610	400	30000

Sulfonamides are one of the oldest antibiotics groups that is still widely used [6]. All substances from this group have been detected in WWTPs effluents, surface water and groundwater, as well as in drinking water [10]. Sulfamethoxazole is the most often detected sulfonamide in the environment [6,10,23]. It is usually prescribed together with trimethoprim to treat various infectious diseases in humans [10,25,26]. Fluoroquinolones are also very often found in water bodies, especially ciprofloxacin. Hydrophilic properties of this antibiotic class make them highly mobile in the aquatic environment. This, together with their high consumption both in human and veterinary medicine, contributes to wide occurrence of ciprofloxacin, from WWTP effluents to drinking water [6,27,28]. Sulfamethoxazole, trimethoprim and ciprofloxacin have been identified in hospital wastewater with concentrations up to 35.5 µg/L [17,29,30]. Besides, sulfanomides and fluoroquinolones have demonstrated very high toxicity of aquatic organisms, especially to cyanobacteria, freshwater algae and duckweeds [10]. These organisms play a crucial role in aquatic ecosystems [10], and therefore whole ecosystems can be disturbed when antibiotics are released into them [31]. Such a wide spreading of these antibiotics resulted in adding ciprofloxacin to the second EU watch list of substances for union-wide monitoring in the field of water policy (EU Decision, 2018/840 of June 5, 2018), and sulfamethoxazole and trimethoprim were selected to be included in the third watch list [32].

1.3. Antimicrobial Resistance as a Global Health Crisis

The presence of antibiotics in natural aquatic environments raises many concerns, first of all because of the development of antimicrobial resistance (AMR). If such pharmaceuticals are continuously released into water bodies, bacterial populations undergo selective pressure and therefore develop antimicrobial resistance in order to survive (Figure 3) [1,14]. This is an adaptive genetic trait of bacterial populations, enabling them to resist the effect of the drug that used to successfully kill or inhibit these microorganisms [1,2,33]. The misuse and overuse of antibiotics in human medicine, as well as inappropriate and frequent use of antibiotics as therapeutics and growth promoters in animal farming, contribute to the development and wide spread of antibiotic resistance [34].

The fast development and spread of resistance to antibiotics is a significant health issue because it affects the ability to treat various infections [5]. Antibiotic resistance to most of the common antibiotics has already been developed, and even last-generation antibiotics have become less effective to treat bacterial infections [10,14]. Thus, the shortage of treatment options develops [14]; higher medical costs are required to create new antibiotics; and mortality increases [10]. Antibiotic resistance is a global health crisis with an enormous potential for health and economic consequences [1]. Currently, 700,000 deaths per year are associated with antibiotic-resistant infections, but it is estimated that this number could increase to 10 million per year by 2050 [1,35].

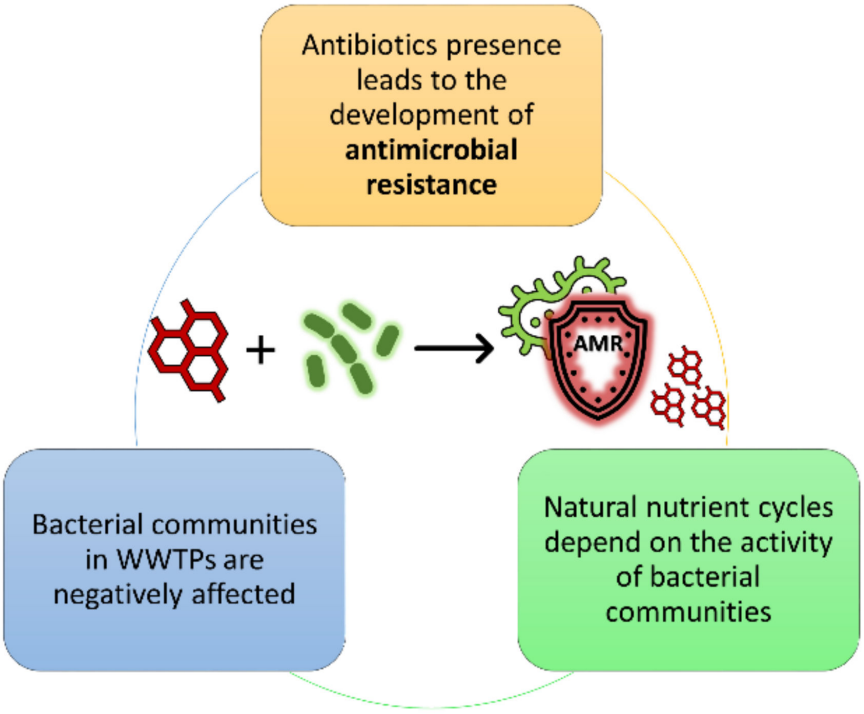

Figure 3. Concerns associated with antibiotics presence in the aquatic environment.

Therefore, each time that antibiotics are released into the natural environment, it contributes to the development of antimicrobial resistance in microorganisms and thus the spread of antibiotic resistant bacteria (ARB) and antibiotic resistance genes (ARGs). ARGs are contaminants of emerging concern, and they are not commonly monitored in the environment. However, they have strong potential in leading to negative ecological and human health effects [16,36]. Unfortunately, there are no legal regulations that define permitted levels of antibiotics or ARB and ARGs allowed to be released into the environment [2,16,17].

1.4. Pathways of Antibiotics Release into Aquatic Environment

Discharge of antibiotics into the natural aquatic environment occurs as a result of (1) industrial production of antibiotics; (2) consumption and excretion of antibiotics by humans and animals; (3) improper disposal of unused or expired antibiotics [1]. Hotspots of antibiotic discharge in the environment include wastewater treatment plants (receiving effluents from households and hospitals), antibiotic manufacturing plants, agriculture and aquaculture (Figure 4) [1,6,9,16]. Disposed antibiotics from households and hospitals end up in landfill, where they can eventually leak to pollute ground water. The usage of farming animal manure and WWTP sludge contaminated with antibiotics as fertilizer also results in the occurrence of antibiotics in ground water [1]. This is because 30 to 90% of oral antibiotic doses taken both by humans and animals are excreted in its unmetabolized form [1,6,17]. This means that antibiotics can be released into the environment as entirely biologically active substances [37,38]. In groundwater, under anoxic conditions, antibiotics remain unchanged for a very long time or might undergo minor degradation and produce even more toxic metabolites [6]. The consumption of groundwater (most often used as a source of drinking water) contaminated with antibiotics, ARB or ARGs might lead to the development of antibiotic resistance in humans [6]. Industrial and agricultural runoff (rainfall and snowmelt runoff) also results in antibiotic occurrence in natural water bodies [2,8,13,39].

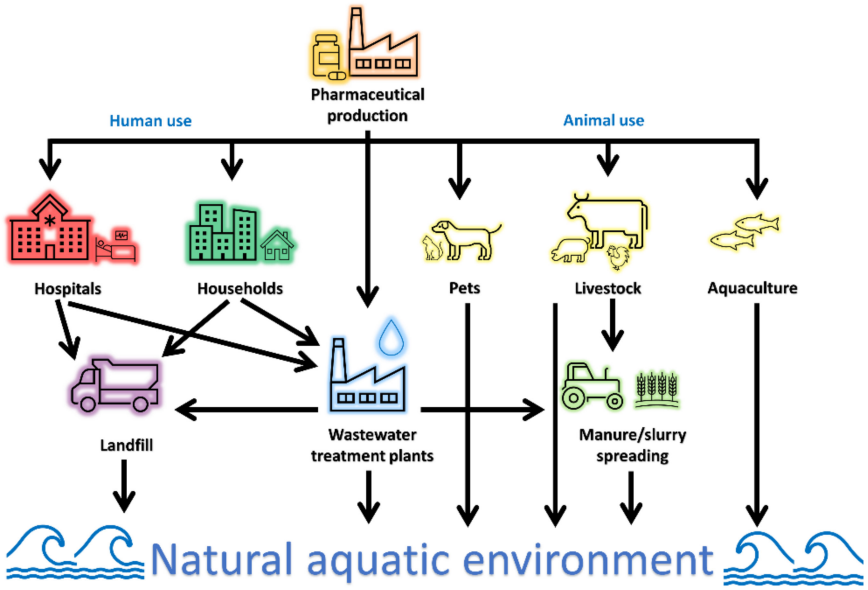

Figure 4. Pathways of antibiotics release into the environment.

Wastewater treatment plants are often recognized as the main source of pharmaceuticals discharge into the environment [37,40]. The reason for this lies in the common design of WWTPs.

Wastewater treatment at WWTP usually comprises a combination of physical, chemical and biological treatment processes. First, physical methods are utilized: large sediments, grit and grease are removed during pre-treatment and primary treatment stages using physical barriers and gravity forces [35]. Physical processes include, for example, sedimentation, flocculation, filtration, etc. [35,41,42]. Afterwards, secondary treatment place-biological processes are employed in order to remove organic content [35,39,42] through aerobic and anaerobic processes. For this purpose, biological reactors are utilized, in which the biochemical degradation of organic substances takes place in a similar way to the one occurring in natural aquatic systems [35]. Biological processes employ various microorganisms (bacteria, fungi, algae) and plants to transform biodegradable organic substances into simple products [41,42]. Biological methods utilize biomass in different forms: sus-

pended (activated sludge), fixed (trickling filters) or suspended in aquatic systems (aerated lagoons) [35,42]. Tertiary treatment takes place in exceptional cases, only when additional water purification is required; for example, the disinfection or removal of specific nutrients or toxic compounds [35]. For this purpose, different chemical and physical methods are used: chlorination (most often), ozonation, UV treatment, membrane filtration, adsorption processes [35,43].

Although common treatment processes are very efficient to remove suspended solids, biodegradable organic compounds, inorganic matter and pathogens, they fail to remove pharmaceuticals and antibiotics, in particular [1,35,44,45]. Biological treatment, which is the foundation of any WWTP, is simple and easy to operate, cost-effective and does not generate toxic by-products [39,41,46]. However, the degradation efficiency of non-biodegradable antibiotics by this method is low [41,42,45–47]. Additionally, what is worse, antibiotics present in wastewater are able to change the composition of microbial communities in bioreactors [8,35] and make bacteria there multi-resistant to antibiotics. As a result, discharge from WWTPs containing antibiotic resistant bacteria and genes, contributes to the wide spread of AMR in the aquatic environment. This poses a significant threat to human health if receiving water bodies are used as a source of drinking water or for recreational purposes [48].

In this review, different advanced water treatment techniques, which are capable of the effective removal of antibiotics when applied in WWTP, are briefly introduced and compared. Among them, various advanced oxidation processes are analyzed, and heterogeneous photocatalysis is highlighted. The fundamentals and mechanism of heterogeneous photocatalysis over TiO_2 are discussed in detail. Surface modification strategies of TiO_2 nanomaterials in order to improve their photoactivity are presented. With this in view, the focus of the present review is on the removal efficiency of SMX, TMP and CIP from the aqueous environment by photocatalysis over various recently developed unmodified and modified TiO_2 materials. The role of different operating parameters on the removal efficiency is outlined. The ecotoxicity of the final products is also considered. Finally, further research needs are presented. We expect that the present review will provide some new ideas for the design and development of TiO_2-based photocatalysts to be successfully applied in antibiotics elimination from the aquatic environment.

2. Water Treatment Techniques for Degradation of Antibiotics

It is clear from the previous section that conventional wastewater treatment plants have not been designed to eliminate pharmaceuticals from wastewater, and therefore they are unable to provide the efficient treatment of water contaminated with antibiotics [35,41,46,47,49]. Therefore, the application of advanced water treatment technologies is required in order to achieve the effective removal of pharmaceuticals in aqueous systems. Among these technologies, adsorption, membrane filtration and advanced oxidation processes gain a lot of interest. Short descriptions, advantages and drawbacks are compiled in Table 3.

Table 3. Advanced technologies applied to the treatment of wastewater contaminated with antibiotics.

Technology	Description	Advantages	Drawbacks
Adsorption	A mass transfer process of accumulation of chemicals from the liquid phase into the solid phase of adsorbent [23,42]. A wide variety of adsorbents is utilized (clays and minerals, metal oxides, polymers, nanocomposites, carbon nanotubes; activated carbon and biochars are among the most commonly used) [23,46].	High removal efficiency [35,45,47] Short treatment period and simple operation [43,46] Low operation costs [23,41]	Complex and expensive production of some adsorbents [46] High material costs and high regeneration costs of the used adsorbent [23,43,47] Nondestructive process, production of secondary waste [35,41,47]
Membrane filtration	Physical process of chemicals separation using synthetic membranes [42]. Only nanofiltration and reverse osmosis can be efficiently applied to antibiotics removal [46].	High removal efficiency [42,45] Fast and simple process with no chemicals involved [50,51]	High costs of operation and maintenance [35,43] Membrane fouling [50,51] Not suitable for large volumes of wastewater [45,51] Nondestructive process [41,45]
Advanced oxidation processes (AOPs)	Processes based on utilization of highly reactive chemical species that are efficient in oxidizing and mineralizing organic compounds [35,41].	High efficiency of pollutants degradation and possibility of complete mineralization in a short period of time [43,46,47] Include environmentally friendly, safe and sustainable processes [52] Disinfection properties [43]	High operation costs [43,46]. In case of incomplete mineralization post-treatment is required to remove toxicity [43]
AOPs: Ozonation	Ozone molecule O_3 has high oxidation capability (E_0 = 2.07 V), and therefore is able to efficiently oxidize organic pollutants [41,42].	On-site generation of ozone [43] No waste production [49]	High operation and energy costs [45,47,49] Possible formation of harmful by-products [35,46,47] Limited pollutant mineralization [43]
AOPs: Fenton process (homogeneous)	Fenton reagent consisting of Fe^{2+} and H_2O_2 produces highly reactive hydroxyl radicals $^{\bullet}OH$ that oxidize organic pollutants [49,53].	Fast, effective and safe process [42,49] Easy operation [53] Possible mineralization of pollutants [43] Iron is abundant and non-toxic [42,49]	Reaction is limited to acidic conditions pH 2.8–3.5 [41,43,53] Large volumes of ferrous sludge produced [42,43,53] Complicated recovery of Fe^{2+}/Fe^{3+} ions [23]

Table 3. *Cont.*

Technology	Description	Advantages	Drawbacks
AOPs: Electrochemical processes	Processes of oxidizing organic substances using electric current [53]. Most widely employed anode materials include graphite and TiO_2, as well as Ti-based alloys, Ru and Ir oxides [41].	Easy to operate, safe and highly efficient process [23,43] No chemical reagents required and no generation of secondary wastes [23,41] Suitable for waste waters with high concentrations of pharmaceuticals [45]	High operation costs [23,42,45] Expensive electrodes [41], short electrode life time, electrode fouling [23] It is required that wastewater is highly conductive (otherwise electrolytes should be added) [23,41,42] Mass transfer resistance [41] Applicable to wastewater with low flow rate [45] Water oxidation occurs faster than oxidation of organic pollutants [42]
AOPs: Ultrasonication	Processes employing sound waves for formation, growth and collapse of bubbles in liquid media [23].	No chemical reagents required [43]	High operation costs [43] Destruction and corrosion of reactor metallic surface [23]
AOPs: Radiation assisted catalytic reaction	Processes employing electromagnetic radiation (for example, microwaves, x-rays, gamma rays) to form highly reactive species ($^{\bullet}OH$, e^-, $^{\bullet}H$, H_2, H_2O_2, H_3O^+) that oxidize organic pollutants [23,53].	Fast and energy-efficient process [23] No chemical reagents required [23]	Toxicity of intermediates in mineralization process should be considered [23] Various factors affect degradation efficiency (dose of radiation, pH, water matrix composition) [51]
AOPs: Catalytic wet peroxide oxidation	Processes of pollutants degradation in aqueous media through catalytic H_2O_2 reduction to OH^- and $^{\bullet}OH$ under extreme pressures and temperatures [42].	Fast and efficient process [23]	High operation and material costs [23] Some substances (containing nitro functional groups and halogens) are difficult to degrade [42]
AOPs: Photolysis	Processes employing light (artificial or natural) for the generation of reactive species and subsequent degradation of organic pollutants [41].	Cost-effective process [41]	Lowest degradation efficiency among AOPs [45] Applicable only to photo-sensitive pollutants [41]

Table 3. *Cont.*

Technology	Description	Advantages	Drawbacks
AOPs: Photocatalysis	Degradation of organic contaminants using semiconducting materials (photocatalysts) and light (artificial or natural) [42].	Easy to operate, highly efficient and environmentally friendly process [18,42,51] Performed under ambient temperature and pressure and utilizes atmospheric oxygen as oxidant [23,44] Complete mineralization of organic pollutants is possible, no waste generation [42,43] Efficient recovery and reuse of photocatalysts is possible [52,54]	Fast recombination of photogenerated charge carriers decreases process efficiency [42] Limited visible light response [42] Laboratory scale [43] Not applicable to water with high concentrations of organic pollutants [42,51] Losses of photocatalyst under long-term operation [51] Toxicity of by-products should be considered [42]

As follows from the information in Table 3, physical processes, such as adsorption and membrane filtration, have one significant limitation—the production of secondary waste. The problem is that pollutants are transferred from the liquid phase of wastewater to the solid phase of adsorbents in the case of adsorption process, or are collected on the membrane surface in the case of membrane filtration without any decomposition [44]. This means that pharmaceuticals do not undergo any changes in chemical structure and therefore, still retain their harmful potential [35]. Moreover, the obtained waste should be properly disposed of, which makes a treatment technology more expensive. Thus, the main advantage of advanced oxidation processes is the obvious, efficient degradation of pollutants with the possibility of their complete mineralization.

Currently, AOPs are widely studied by different research groups, as these methods give very promising results and have high potential for broad application. Carried out studies state that the best performance is associated with the antibiotic removal strategies that involve combined processes [41,46]. They include, for example, a combination of AOPs with biological treatment [43,57] or membrane filtration [42,57]. However, further improvements are needed, mainly in the development of new materials for AOPs [46], in order to make these processes cost-effective while retaining high efficiency.

2.1. Advanced Oxidation Processes

Advanced oxidation processes (AOPs) are powerful technologies used in wastewater treatment to degrade organic pollutants, including various pharmaceuticals [58]. Most common AOPs include the Fenton process, heterogeneous photocatalysis, ozonation, electrochemical oxidation, etc., and are briefly described and compared in Table 3. As can be seen from the table, AOPs include many different processes, and the only feature that unites all of them is the production of highly reactive species, for example, hydroxyl radicals ($^{\bullet}OH$), ozone molecules (O_3), superoxide radicals ($O_2^{\bullet-}$), hydrogen peroxide molecules (H_2O_2), etc.

The efficient generation of hydroxyl radicals ($^{\bullet}OH$) in situ is the purpose of AOPs, as it defines their performance. These radicals are the second highest powerful species after fluorine with oxidizing potential E_0 = 2.80 V [52,55]. $^{\bullet}OH$ radicals attack organic molecules rapidly and non-selectively, oxidizing them and thus transforming them into more biodegradable and less toxic substances. What is more, $^{\bullet}OH$ radicals are also capable of mineralizing organic contaminants, yielding CO_2, H_2O and inorganic ions. In this case, organic pollutants are completely destroyed and therefore no further post-treatment is required.

The combination of different AOPs is gaining lots of interest due to enhanced process efficiency. For example, the performance of homogeneous Fenton reaction, being the most widely applied AOP [55], can be significantly increased through combination with UV light (photo-Fenton [23,41]), with electrochemical process (electro-Fenton [55]), or even with both (photo-electro-Fenton [42]).

After Fenton process, heterogeneous photocatalysis is the second most widely applied AOP [55]. This technology has numerous advantages over the other types of AOPs, mainly simplicity and sustainability. The possibility of the utilization of solar energy as an abundant, clean and renewable light source makes solar photocatalysis a green and sustainable technology for wastewater treatment. It is also very cost-efficient compared to the technologies utilizing artificial sources of light or electrodes. Besides, it was found that solar photocatalysis-based AOPs have the lowest global warming potential compared to the other wastewater treatment methods [57].

2.2. Heterogeneous Photocatalysis over TiO_2

Heterogeneous photocatalysis employs various semiconducting materials as photocatalysts, for example, metal oxides (TiO_2, SnO_2, Fe_2O_3, WO_3, ZnO, Ag_3O_4 [35,44,53,59]), metal sulfides (ZnS, CdS [44,53]), as well as g-C_3N_4-based materials [56]. Among these, TiO_2 is the most widely utilized photocatalyst due to its unique properties. They in-

clude high physical and chemical stabilities, high photocatalytic activity, nontoxicity, large abundance and low cost [60,61]. Besides, TiO_2 employment is preferred in the form of nanostructures, which have improved surface chemistry and increased surface area [62]. This results in the faster and more efficient mineralization of organic pollutants.

What makes TiO_2 such an effective photocatalyst, is the favorable thermodynamic processes taking place in TiO_2 photocatalysis. It is known that the conduction band (CB) energy of TiO_2 anatase (with a band gap E_g = 3.2 eV) is –0.51 V [63] at neutral pH, while valence band (VB) energy is 2.69 V under the same conditions. This means that CB energy level is more negative than potential of oxygen reduction ($E_0(O_2/O_2^{\bullet -}) = -0.33$ V), and that VB energy level is more positive than the potential of water oxidation ($E_0(H_2O/^{\bullet}OH)$ = 2.29 V). This makes it possible to obtain highly reactive oxidizing species-superoxide radicals $O_2^{\bullet -}$ and hydroxyl radicals $^{\bullet}OH$ in photocatalytic process over TiO_2, which non-selectively degrade and mineralize organic pollutants.

In general, a photocatalytic process over TiO_2 comprises the following stages [62,64]:

1. Adsorption of organic pollutants on TiO_2 surface;
2. The photocatalytic degradation of the adsorbed organic pollutants via oxidation-reduction reactions with photogenerated electrons, holes and reactive species (depicted in Figure 5);
3. Desorption of degradation products.

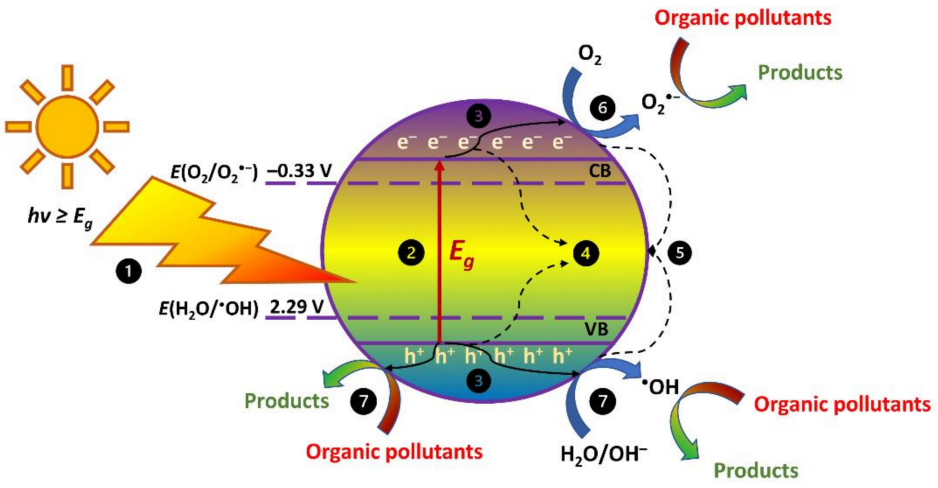

Figure 5. Photocatalytic process over TiO_2: (**1**) Photon absorption; (**2**) Generation and separation of electron-hole pairs (e^- and h^+); (**3**) Transport of electrons and holes in the bulk to the photocatalyst surface; (**4**) Recombination of electrons and holes in the bulk; (**5**) Surface recombination of electrons and holes; (**6**) Reduction reaction on TiO_2 surface; (**7**) Oxidation reactions on TiO_2 surface.

Therefore, photocatalytic process itself is initiated when TiO_2 absorbs a photon from the light source with the energy (hv), equal to or greater than the band gap (E_g) of the photocatalyst [65]. This makes the photocatalyst electrons e^- excited, so that they move from the valence band to the conduction band, and holes h^+ are generated in the valence band (Equation (1)) [45,54].

$$TiO_2 + hv \rightarrow e^-_{CB} + h^+_{VB} \text{ (if } hv \geq E_g) \quad (1)$$

After excitation, separated charge carriers (e^- and h^+) might recombine in the bulk with an energy release (Equation (2)) [45]. Otherwise, they migrate to the surface of TiO_2, where they participate in redox reactions with organic pollutants previously adsorbed on

the photocatalyst surface. The recombination of the charge carriers on the catalyst surface might also take place.

$$e^-_{CB} + h^+_{VB} \rightarrow \text{energy} \quad (2)$$

Photogenerated holes have high oxidizing ability: they degrade organic compounds directly or oxidize water, so that hydrogen ions (H^+) and hydroxyl radicals ($^\bullet OH$) are generated (Equation (3)) [18,53].

$$h^+_{VB} + H_2O \rightarrow H^+ + {}^\bullet OH \quad (3)$$

Besides, holes oxidize OH^- at the catalyst surface, and more $^\bullet OH$ radicals are produced (Equation (4)).

$$h^+_{VB} + OH^- \rightarrow {}^\bullet OH \quad (4)$$

$^\bullet OH$ radicals being very powerful oxidizing species degrade organic pollutants to carbon dioxide and water (Equation (5)) [54].

$$^\bullet OH + \text{organic pollutants} \rightarrow CO_2 + H_2O \quad (5)$$

Photogenerated electrons, in turn, have high reducing ability. Thus, electrons react with O_2 to form superoxide radicals $O_2^{\bullet -}$ (Equation (6)) [18,53].

$$e^-_{CB} + O_2 \rightarrow O_2^{\bullet -} \quad (6)$$

These superoxide radicals react with hydrogen ions (H^+) and generate hydroperoxyl radicals $^\bullet HO_2$ (Equation (7)), which further produce hydrogen peroxide H_2O_2 (Equation (8)).

$$O_2^{\bullet -} + H^+ \rightarrow {}^\bullet HO_2 \quad (7)$$

$$^\bullet HO_2 + {}^\bullet HO_2 \rightarrow H_2O_2 + O_2 \quad (8)$$

Hydrogen peroxide H_2O_2 might react with superoxide radicals $O_2^{\bullet -}$ (Equation (9)) or is decomposed by the light (Equation (10)), and $^\bullet OH$ radicals are produced in both cases.

$$H_2O_2 + O_2^{\bullet -} \rightarrow {}^\bullet OH + OH^- + O_2 \quad (9)$$

$$H_2O_2 + h\nu \rightarrow {}^\bullet OH + {}^\bullet OH \quad (10)$$

Generated reactive species ($O_2^{\bullet -}$, $^\bullet HO_2$) are capable of degrading and mineralizing any organic compounds to CO_2 and H_2O (Equations (11) and (12)) [51,66].

$$O_2^{\bullet -} + \text{organic pollutants} \rightarrow CO_2 + H_2O \quad (11)$$

$$^\bullet HO_2 + \text{organic pollutants} \rightarrow CO_2 + H_2O \quad (12)$$

In TiO_2 photocatalysis, the oxidation of organic substances might take place either through aliphatic oxidation ($^\bullet OH$ radicals remove H^+ from the molecule), or through aromatic oxidation (O_2 and $O_2^{\bullet -}$ oxidize aromatic molecule) [62].

2.3. Doping and Modification of TiO_2

Although TiO_2 has high photocatalytic activity, there are two main drawbacks limiting its wide practical application [67,68]. These limitations include unfavorable dynamics of photogenerated charge carriers (fast recombination of electrons and holes in bulk and on the photocatalyst surface) and poor visible light harvesting [63]. Wide band gap of TiO_2 (3.0–3.2 eV [63]) limits TiO_2 usage to UV light only (wavelengths shorter than 390 nm) according to Equation (13) [63]:

$$\lambda = \frac{h \times c}{E_g} \approx 390\ nm, \quad (13)$$

where h is the Planck constant, c is the speed of light, E_g is the band gap of the photocatalyst (3.2 eV for TiO_2 anatase) [63].

It is known that UV light accounts for only 3–5% of the solar light, while visible light constitutes 45% of the solar spectrum [18,54]. It is very important that process is cost-effective and sustainable when implemented on an industrial scale. If heterogeneous photocatalysis over TiO_2 cannot be carried out under visible light, expensive UV light sources have to be used [18,44]. It is obvious that for successful TiO_2 employment under visible light, the wavelength adsorption of the photocatalyst should be extended into the visible region, thus making TiO_2 active in visible light [44,66].

Therefore, in order to prevent the recombination of electrons and holes and ensure the effective utilization of visible light, particular measures should be taken. The separation of charge carriers should be enhanced, their lifetime should be prolonged, photocatalyst band gap should be narrowed and TiO_2 surface area should be increased [63,69]. For this purpose, various strategies of TiO_2 surface modification have been proposed [55]. They include mainly metal and non-metal doping [18,44,54,70], metal and non-metal co-doping [44], coupling with other semiconductors [18,44,66], constructing heterojunctions [54,63] and Z-schemes [45], dye sensitization [44].

In metal doping, metal ions (transition metals, noble metals, rare earth metals) [18,69] substitute for Ti^{4+}. This suppresses electron-hole recombination, effectively reduces the photocatalyst band gap, enhances visible light harvesting and improves photocatalyst surface morphology [18,45,71]. Nonmetal dopants (N, C, S, B, F) also reduce the band gap and are stated to be more effective in making TiO_2 active in visible light [18,71]. In co-doping, TiO_2 is doped with two or more metals, nonmetals or both metals and nonmetals, in order to overcome the limitations of a single-doped photocatalyst [18].

Coupling TiO_2 with another semiconductor (SnO_2, ZnO, SiO_2, CdS) to obtain heterojunctions also contributes to the better separation of the charge carriers and improves utilization of visible light [18,45,64]. In the case of Z-scheme photocatalysts, band structure remains similar to the one of heterojunctions. However, the transfer mechanism of electrons and holes changes. In particular, recombination of the charge carriers with weaker redox abilities take place, while electrons and holes with stronger redox abilities are separated and preserved [45]. Another way to enhance the separation of electrons and holes is to create vacancy engineered photocatalysts containing crystal defects-oxygen vacancies. Thus, a new energy level is formed between the valence band and conduction band and, as a result, band gap is reduced, and visible light response is improved [45]. Dye-sensitized photocatalysts are also used to generate more electrons and therefore enhance photocatalytic performance [70,71].

Still, there are many other parameters affecting the efficiency of the photocatalytic degradation process; for example, organic pollutant concentration, photocatalyst dosage, light intensity, pH of reaction solution, etc. [51]. Thus, process conditions should be properly designed, numerously tested and optimized, so that maximum performance can be achieved while keeping costs to a minimum.

3. Parameters Affecting Efficiency of Photocatalytic Degradation over TiO_2-Based Photocatalysts

3.1. Effect of Antibiotic Concentration

The initial concentration of a contaminant is a very important parameter in a photocatalytic process. Researchers study its effect on the photodegradation of pharmaceuticals by varying the initial concentration of target antibiotics under other similar conditions.

The effect of initial concentrations of SMX was studied by Tiwari et al. [72] in photocatalytic removal over thin film photocatalyst Ag0(NP)/TiO_2(B). Researchers reported a decrease in photodegradation efficiency from 57% to 20% when SMX concentration was increased from 0.5 mgL^{-1} to 15.0 mgL^{-1}.

A similar inverse relationship between the photodegradation efficiency and antibiotic concentration was observed and reported by Alfred et al. [73], Ioannidou et al. [74], Cai and

Hu [75], Sarafraz et al. [24], Karim and Shriwastav [76], Wu et al. [77] and Hassani et al. [78], who used different photocatalyst systems for removal of different target antibiotics.

Researchers attribute the hindered decomposition of pharmaceuticals when antibiotic concentration is increased to a number of reasons. First of all, higher contaminant concentration means that higher number of contaminant molecules are adsorbed on active sites of the photocatalyst [75,77]. As a result, generation of reactive species is suppressed [75]. Secondly, as antibiotic concentration increases, more byproducts and intermediates are produced that compete with antibiotic molecules for a limited number of active sites on photocatalyst surface and reactive species present [24,73,77,78]. In addition, solution transmittance might be reduced when pharmaceutical concentration in the solution is increased. Weaker transmittance results in longer pathways for photons to get to photocatalyst, so that lower number of photons is adsorbed on photocatalyst surface and, therefore, a lower number of reactive species are generated [77,78]. Moreover, some antibiotics (for example, CIP) adsorb photons themselves, so that a lower number of photons are available for the photocatalyst [24].

3.2. Effect of Catalyst Concentration

The influence of photocatalyst concentration on removal efficiency of different antibiotics has been studied by many researchers. For example, Xie et al. [79] performed photocatalytic experiments under visible light irradiation utilizing different concentrations of a photocatalyst (Zn-TiO_2/pBC): 0.625 gL^{-1}, 1.25 gL^{-1} and 2.5 gL^{-1}. The optimal concentration was found to be 1.25 g, resulting in 81.21% (k_{app} = 0.0087 min^{-1}) removal efficiency of 10 mgL^{-1} SMX after 3 h of irradiation. For comparison, 0.625 gL^{-1} and 2.5 gL^{-1} catalyst concentrations could achieve 57.73% (k_{app} = 0.0043 min^{-1}) and 76.28% (k_{app} = 0.0075 min^{-1}) SMX degradation under the same conditions, respectively. The same results were obtained previously by Zhang et al. [80] who tested TiO_2/pBC photocatalyst for SMX removal under the same conditions but utilizing UV light instead of visible.

Obviously, increased catalyst concentration results in improved photocatalytic performance only up to a point, and any catalyst dosage beyond the optimal value leads to a decrease in removal efficiency. Such results were obtained also in the works of Ioannidou et al. [74], Kim and Kan [81], Chiang and Doong [82], Sarafraz et al. [24], Karim and Shriwastav [76], Hassani et al. [78] and Abellan et al. [83].

Researchers explain this phenomenon as follows: an increase in photocatalyst concentration increases the number of active sites available on the catalyst surface [82]. A higher number of active sites absorb more photons and, as a result, a higher number of reactive species (for example, hydroxyl radicals) are produced, which take part in antibiotic mineralization [24,74,79]. As a result, higher antibiotic removal and process efficiency can be achieved. However, excessive catalyst dosages limit the utilization of light because of greater photocatalyst aggregation and increased turbidity of the reaction solution [78–80]. The first one leads to a decrease of the catalyst active surface area, while the latter, to the reduced penetration of light through the light scattering effect [24,76,80,82]. This results in the generation of smaller number of reactive species and, therefore, photocatalytic efficiency decreases.

However, the situation is the opposite when it comes to mineralization efficiency. Kim and Kan [81] studied the effect of biochar/TiO_2 catalyst concentration (2.5–10 gL^{-1}) on the removal efficiency of 0.1 L SMX solution (10 mgL^{-1}). Although increased catalyst dosage led to a slight decrease in photocatalytic SMX removal from 86% to 76%, COD removal efficiency improved from 35% to 65%. Authors explain this phenomenon as follows: SMX can be better degraded by photolysis in UV-C light (SMX absorbs light at 250–270 nm [81,84]), than by photocatalysis. High photocatalyst loading results in high UV light absorption on TiO_2 surface. As a result, interaction between UV light and SMX decreases, and therefore photolysis efficiency also decreases. However, higher photocatalyst dosage contributes to the enhanced generation of $^{\bullet}OH$ radicals and, therefore, significantly improves COD removal efficiency that is impossible under photolysis only.

The same conclusions were drawn by Nasuhoglu et al. [85], Gong and Chu [86] and Choi et al. [87].

3.3. Effect of pH

pH plays a very important role in the photocatalytic decomposition of organic pollutants. Its change affects the concentration of H^+ and OH^- ions in a solution [88], which has a direct influence on the generation of reactive species (photogenerated holes h^+, hydroxyl radicals $^\bullet OH$, superoxide radicals $O_2^{\bullet -}$) and surface chemistry (surface charge of photocatalyst, reactivity of pollutants and electrostatic interaction between pollutants and photocatalyst) [76,77,88].

Photocatalysis efficiency greatly depends on the surface properties of the photocatalyst. The surface charge of TiO_2 in aqueous solutions depends on the solution pH and zero-charge point of TiO_2. The point of zero charge (pH_{PZC}) is pH at which catalyst surface is uncharged and is calculated as follows [63]:

$$pH_{PZC} = 1/2\ (pK_{a1} + pK_{a2}) \quad (14)$$

$$Ti\text{-}OH_2^+ \leftrightarrow Ti\text{-}OH + H^+\ (pK_{a1}) \quad (15)$$

$$Ti\text{-}OH \leftrightarrow Ti\text{-}O^- + H^+\ (pK_{a2}) \quad (16)$$

pH_{PZC} of TiO_2 P25 is reported to be ~6.2 (pK_{a1} = 4.5 and pK_{a2} = 8) [63]. Thus, TiO_2 is positively charged at pH < 6.2 and negatively charged at pH > 6.2 [75].

Alfred et al. [73], Wang et al. [89], Yuan et al. [84], Xie et al. [79], Tiwari et al. [72], Zhang et al. [80], Cai and Hu [75] studied the influence of pH on the photocatalytic degradation of SMX and observed decrease in SMX removal efficiency with an increase in initial pH. For example, the kinetic parameters of SMX photocatalytic degradation gradually decreased from k = 0.0087 min^{-1} to k = 0.0049 min^{-1} when pH increased from 5.03 to 10.97, respectively [79]. This can be explained when the ionic states of both pharmaceutical compound and photocatalyst are considered. The pK_a values of SMX are reported to be as follows: pK_{a1} = 1.85 ± 0.30 and pK_{a2} = 5.60 ± 0.04 [75,84]. It means that SMX exists in cationic form when pH < 1.85, in anionic form when pH > 5.6, and in neutral form when 1.85 < pH < 5.6. When SMX and TiO_2 surfaces are both positively or negatively charged, there is no electrostatic attraction between them. As a result, adsorption cannot contribute to SMX removal, and only photocatalytic degradation takes place [90]. Besides, when initial pH is close to pH_{ZPC} of photocatalyst, catalyst aggregation might occur, resulting in reduced surface area and decreased photodegradation efficiency [84]. Results suggest that the neutral form of SMX (pH 3–5) is more easily photodegraded than its charged species [73,75], as SMX shows stronger light absorption and higher photochemical reactivity in its neutral form [84].

On the contrary, Mourid et al. [90] and Dlugosz et al. [91] reported higher rates of photocatalytic SMX removal at higher pH than at lower pH. Such contradicting results of pH effect on SMX photocatalytic removal demonstrate importance of taking into account the role of reactive species. When the main reactive species in the degradation process are holes (h^+), low pH values favor efficiency of photocatalytic decomposition [89]. On the other hand, if the main reactive species are $^\bullet OH$, then an increase in pH leads to an $^\bullet OH$ content increase and, therefore, enhances photodegradation efficiency [84,89,90]. For example, in their research, Wang et al. [89] found that h^+ played major role in the photocatalytic degradation of SMX, while de Matos Rodrigues et al. [92] reported $^\bullet OH$ and $O_2^{\bullet -}$ to be the main reactive species in SMX decomposition. This clearly demonstrates that all the experimental conditions should be considered in order to evaluate the pH effect on SMX photocatalytic removal.

Cai and Hu [75] found that the photocatalytic removal rate of TMP (pK_a = 6.7) was almost similar at pH 3, 5, and 9 (~90%) and lower at pH 7 (68%). The authors attributed such a performance to the effect of pH on the absorption spectrum of the antibiotic. Luo et al. [93] also did not observe any significant influence of pH on TMP photodegradation.

The influence of pH on the decomposition rate of CIP was studied by Sarafraz et al. [24] who carried out photocatalytic degradation of CIP at initial pH of 4, 5.5, 7, 8.5 and 10 and obtained the following kinetic parameter values: 0.0237, 0.0417, 0.0763, 0.028 and 0.0196, respectively. The highest removal rate of CIP was observed at pH 7. A similar trend (increase in removal efficiency with pH increase up to a point and a subsequent decrease in efficiency with further pH increase) was also reported by Hu et al. [94] (highest efficiency at pH 6.3), Karim and Shriwastav [76] (highest efficiency at pH 7), Hassani et al. [78] (highest efficiency at pH 5), Gad-Allah et al. [95] (highest efficiency at pH 5.8). Such results can be explained by the ionic values of CIP and the surface charge of different photocatalyst used. It is known that CIP has two pK_a values: pK_{a1} = 5.9 and pK_{a2} = 8.9 [24,77,78]. It means that CIP is present in cationic form CIP^+ when pH < 5.9, in zwitterionic form $CIP^{\pm}$ when 5.9 < pH < 8.9 and in anionic form CIP^- when pH > 8.9 [24,77]. If TiO_2 with pH_{PZC} = 6.2 is used as a photocatalyst, then, in alkaline conditions when both TiO_2 surface and CIP are charged negatively (in acidic conditions, both charged positively), electrostatic repulsion occurs between them, decreasing removal efficiency [24,78,94]. Results obtained in the abovementioned studies demonstrated that photocatalytic decomposition efficiency was significantly improved at neutral pH, when CIP was present in its zwitterionic form [24,76]. Besides, predominant reactive species in the process should also be taken into account [77]. Sarafraz et al. [24], Hu et al. [94], Li and Hu [96] found that h^+ and $^{\bullet}OH$ played a major role in the CIP degradation process. At the same time, Li et al. [97], Huang et al. [98] and Du et al. [99] confirmed h^+ and $O_2^{\bullet-}$ to be the main reactive species, while Gan, Zhang and Xiong et al. [100] reported all three radicals (h^+, $^{\bullet}OH$ and $O_2^{\bullet-}$) to play a significant part in CIP photocatalytic decomposition.

3.4. Effect of Presence of Inorganic Ions

Inorganic anions naturally present in water bodies have a significant impact on the photocatalytic removal of organic pollutants. Their presence affects both working pH and ionic strength of a reaction solution that eventually leads to the change in concentration of active sites on the photocatalyst surface, catalyst adsorption capacity and electrostatic interaction between organic molecules and the catalyst surface [84]. Besides, inorganic anions compete with antibiotic molecules for the same active sites on the photocatalyst surface [79,84]. These anions are also able to react with reactive species-photogenerated holes and hydroxyl radicals, decreasing their amount in the system. When h^+ are captured by inorganic anions, the production of $^{\bullet}OH$ is hindered and, therefore, the decomposition rate of antibiotics decreases [24,78,79,89]. The presence of some inorganic ions might also result in photocatalyst agglomeration, reducing the photocatalytic efficiency of the process [79].

Yuan et al. [84] studied the impact of five inorganic anions (Cl^-, SO_4^{2-}, HCO_3^-, $H_2PO_4^-$, HPO_4^{2-}) on the photocatalytic removal of SMX over TiO_2 P25. The authors reported the inhibition of SMX oxidation in the order as follows: $HCO_3^- > SO_4^{2-} > Cl^-$ with increased inhibition when concentrations of the anions increased. Thus, k_{app} values decreased from 0.544 (without inorganic anions) to 0.485 (1 mM) and 0.212 (3 mM) when HCO_3^- anions were added; to 0.432 (1 mM) and 0.314 (3 mM) when SO_4^{2-} anions were added; and to 0.530 (1 mM) and 0.501 (3 mM) when Cl^- anions were added. k_{app} value also decreased to 0.416 (0.1 mM) and 0.305 (0.3 mM) when HPO_4^{2-} anions were added. However, when $H_2PO_4^-$ anions were present, a slight improvement in SMX photocatalytic decomposition was observed. k_{app} value increased from 0.544 (without $H_2PO_4^-$ anions) to 0.552 and 0.586 when 0.1 mM and 0.3 mM of $H_2PO_4^-$ anions were added, respectively. Researchers attributed inhibited SMX decomposition to the suppression of reactive species (h^+, $^{\bullet}OH$) by anions. On the contrary, the slightly accelerated removal of SMX in case of $H_2PO_4^-$ addition was attributed to the effect of a phosphorus-containing anion. It was reported to be able to enhance e^- transfer between h^+ and water molecules to form hydroxyl radicals $^{\bullet}OH$ and, therefore, improve SMX decomposition. Similarly, Xie et al. [79] reported the weakened photocatalytic performance of TiO_2 in SMX removal when SO_4^{2-},

Cl^-, NO_3^- were present in the reaction system, and Wang et al. [89] when HCO_3^- anions were added.

Photocatalytic oxidation of ciprofloxacin was affected in a similar way. Sarafraz et al. [24] found that HCO_3^-, SO_4^{2-}, Cl^-, and NO_3^- anions slightly decreased the efficiency of CIP photocatalytic decomposition. Among the studied anions, HCO_3^- anions were reported to cause the most significant inhibitory effect, while Cl^- anions were the least significant. Hassani et al. [78] also assessed the influence of HCO_3^-, SO_4^{2-}, I^-, and Cl^- anions on CIP photocatalytic removal and obtained different results regarding the highest inhibition. Researchers reported a decrease in decomposition efficiency from 61.70% to 52.87%, 42.94%, 39.86% and 25.83%, respectively.

3.5. Effect of Presence of Natural Organic Matter

Natural organic matter (NOM) is widely present in natural water bodies in relatively high quantities (0.1–50 mgL^{-1}) [96]. It consists of different aromatic and aliphatic organic compounds, including humic substances [84,89,96] and negatively affects the efficiency of photocatalytic processes. The photocatalytic decomposition of antibiotics is reduced for a number of reasons. First of all, NOM competes with antibiotic molecules for the same active sites on the photocatalyst surface and for the same number of reactive species ($^{\bullet}OH$, h^+ and $O_2^{\bullet-}$) present in reaction media [84,87,89,96,101]. Secondly, NOM can absorb light both in the UV and visible range that is also harvested by the photocatalyst, thus creating an inner filter effect [84,96,101]. As a result, photocatalyst performance is significantly reduced. However, the inhibitory impact of natural organic matter depends greatly on the type and concentration of NOM, photocatalyst properties and target antibiotics [84,96,101].

Awfa et al. [101] assessed the photocatalytic oxidation of SMX in the presence of NOM using pure TiO_2 P25 and magnetic carbon nanotube-TiO_2 P25 composites (MCNT-TiO_2). Researchers reported the significantly reduced rate constants of SMX removal from 4.7×10^{-2} min^{-1} to 5×10^{-3} min^{-1} over TiO_2 P25; and from 4.9×10^{-2} min^{-1} to 7×10^{-3} min^{-1} over MCNT-TiO_2 in the absence and in the presence of NOM, respectively. Yuan et al. [84] studied the effect of three different types of NOM on SMX photocatalytic decomposition and observed decreased antibiotic removal when NOM concentration was increased. Photodegradation rates of SMX oxidation dropped from 0.544 min^{-1} in the absence of NOM to 0.081–0.141 min^{-1} in the presence of NOM, depending on the NOM type. Similar results were obtained by Li and Hu [96], who observed a negative influence of different NOM isolates on CIP photocatalytic removal. Sarafraz et al. [24] also carried out research on the influence of NOM different concentrations on CIP photocatalytic removal. Researchers reported the inhibition of CIP decomposition rate from 91.5% to 59% when the concentration of NOM was increased from 5 to 30 mgL^{-1}.

3.6. Effect of Reaction Media

At present, antibiotics can be widely found in natural water bodies and different wastewater effluents [79,102]. These water matrices are complex systems—they contain large amounts of organic matter or various inorganic anions that significantly affect photocatalysis efficiency due to the reasons described above [80,103]. Many researchers have carried out studies on the photocatalytic degradation of pharmaceuticals in different water matrices in order to evaluate their inhibitory effect.

Wang et al. [89] studied the photocatalytic degradation of SMX in natural water bodies under solar light. Authors reported decreased removal efficiency (86% in river water and 90.6% in lake water) compared to 100% removal efficiency in deionized water. Inhibited photocatalytic performance was attributed to the presence of organic matter and high turbidity in natural water that resulted in the lower utilization efficiency of the photocatalyst. Xie et al. [79] also observed a significant decrease in photocatalytic degradation of SMX from ~81% in ultrapure water to ~54% in river water under visible light [79]. Carbajo et al. [102] used natural ground water with reduced carbonates to study the photocatalytic degradation of SMX. The values of apparent kinetic constants decreased

from 0.095 min^{-1} in deionized water to 0.061 min^{-1} in natural ground water when the home-made TiO_2 photocatalyst was utilized. Hassani et al. [78] also observed the inhibited photocatalytic decomposition of CIP when well water was used as a matrix.

Porcar-Santos et al. [104] carried out the photocatalytic decomposition of SMX using TiO_2 P25 under simulated solar irradiation, both in deionized water and simulated seawater. As a result, SMX degradation was twice as fast in deionized water than in saline water (pseudo-first order rate constants were 0.041 min^{-1} and 0.020 min^{-1}, respectively). The investigation of the degradation mechanisms revealed a major contribution of reactive halogen species on the photocatalytic degradation of SMX in seawater, while hydroxyl radicals ($^{\bullet}OH$) played their main role in photocatalytic SMX decomposition in deionized water. Yang et al. [105] utilized seawater (34‰ salinity), diluted seawater (20‰ salinity) and distilled water to study the effect of salinity on the photocatalytic degradation of SMX. Authors observed a significant decrease in photocatalysis efficiency with an increase in salinity: the remaining amount of SMX increased from 7.7% in distilled water to 34% in diluted seawater and to 49% in seawater. Apart from that, the inhibitory effect of cations and anions present in seawater was studied and reported to be as follows: $Ca^{2+} > Mg^{2+} > K^{+} > Na^{+}$ for cations, $I^{-} > SO_4{}^{2-} > Cl^{-} > Br^{-}$ for anions. Interestingly, the mineralization rate of the antibiotic was also severely affected. The remaining COD concentration increased from 34% in freshwater experiments to 75% and 84% when salinity was 20‰ and 34‰, respectively.

Malesic-Eleftheriadou et al. [103] carried out photocatalytic experiments with SMX as a target antibiotic using effluent from an urban wastewater treatment plant. The increased complexity of the water matrix resulted in decreased kinetic rates from 0.015 min^{-1} in distilled water to 0.03 min^{-1} in wastewater effluent. Ioannidou et al. [74] studied SMX photocatalytic degradation in three different matrices: ultrapure water, secondary treated wastewater and drinking water. Researchers reported slightly decreased removal efficiency in drinking water (apparent rate constant ~0.1 min^{-1}) and significantly inhibited the photocatalytic process in wastewater (apparent rate constant ~0.015 min^{-1}) compared to the results obtained when ultrapure water was used as a matrix (apparent rate constant ~0.13 min^{-1}). Karim and Shriwastav [76] observed a decrease in CIP photocatalytic removal from 77% to 41% when secondary treated wastewater was used as a matrix instead of distilled water. Large amounts of non-target organic compounds in wastewater effluents consumed reactive species and thus interfered with the photocatalytic decomposition of target antibiotics [74,103].

3.7. Effect of Dissolved Oxygen and Oxidants

The concentration of dissolved oxygen is an important parameter that affects the efficiency of photocatalytic processes. High contents of dissolved oxygen enhance the photocatalytic oxidation of organic pollutants for a number of reasons. First of all, oxygen acts as a trap for photoexcited electrons, decreasing the recombination rate of charge carriers [106]. Secondly, the reaction between oxygen and electrons results in the generation of reactive species: superoxide radicals $O_2{}^{\bullet -}$, hydroxyl radicals $^{\bullet}OH$ and peroxide radicals $^{\bullet}HO_2$ that improve the oxidation rate of pharmaceuticals [107]. As the concentration of dissolved oxygen constantly changes in natural water bodies [90], many researchers have studied its influence on the photocatalytic oxidation of antibiotics.

Mourid et al. [90] studied the effect of dissolved oxygen on SMX removal by carrying out photocatalytic tests in aerated and de-aerated media. The decomposition of the antibiotic decreased from 80% in aerated medium to 45% in de-aerated medium, proving the significance of dissolved oxygen in the photocatalytic process. Diao et al. [107] obtained similar results when CIP was treated under aerobic and anoxic conditions, as removal efficiency was reduced from 97.2% to 56.1%, respectively. The purging of nitrogen (N_2) gas through the reaction system to remove dissolved oxygen was reported by Khan et al. [108] to have an inhibitory effect on the efficiency. CIP photodegradation dropped from 85.91% to 70.98%. Xekoukoulotakis et al. [106] performed photocatalytic tests under two different

conditions. In the first case, an open to air reactor was used, while in the second case, additional oxygen supply was provided. Researchers did not observe a significant influence of mode on CIP photocatalytic degradation. However, mineralization rate was greatly affected, as TOC reduction increased from 76% to 96% when aeration was applied.

The presence of different chemical oxidants can also enhance the efficiency of the photocatalytic process. For example, as Hassani et al. [78] observed in their research, the addition of hydrogen peroxide, potassium iodate and potassium persulfate increased the decomposition efficiency of CIP from 61.70% to 83.36%, 86.43% and 97.88%, respectively. Improved photocatalytic performance was attributed to the increased generation of reactive radicals, mainly $^{\bullet}$OH, through various mechanisms.

3.8. Effect of Light Source

The efficiency of the photocatalytic decomposition of target pharmaceuticals greatly depends on the wavelength of light applied and light intensity [45,88]. An increase in light intensity increases the number of photons in a reaction system. Thus, more charge carriers are generated that take part in photocatalytic oxidation and contribute to an improved removal rate of antibiotics [45]. Taking into account that pure TiO_2 has a band gap of 3.0 eV (rutile phase) and 3.2 eV (anatase phase) [47], it can utilize light in the UV region only (wavelengths below 390 nm) [54]. However, various TiO_2-based photocatalysts can be successfully applied under visible light [109]. Many researchers have studied the performance of TiO_2-based photocatalysts under UV-light [87,110–112], visible light [77,79,113,114], simulated solar light irradiation [94,101,104,115] and natural sunlight [116–118]. Eskandarian et al. [119] studied the photocatalytic removal of SMX using LED lamps emitting light in different ranges of UV: UV-A (365 $\pm$ 10 nm), UV-B (300 $\pm$ 5 nm) and UV-C (260 $\pm$ 10 nm). Researchers reported 58%, 80% and 100% SMX decomposition efficiency after 3 h of irradiation when UV-A, UV-B and UV-C LED lamps were employed, respectively. The mineralization of the antibiotic followed the same trend, increasing from 35.1% (UV-A) to 59.9% (UV-C). An increase in CIP removal efficiency was observed in the same order (UV-A < UV-B < UV-C) by Hassani et al. [78]. Authors attributed such results to the increase in energy of photons emitted. A higher number of reactive species was produced under UV-C light compared to UV-B and UV-A. Lin et al. [120] compared the photocatalytic performance of the synthesized TiO_2-based photocatalysts under UV irradiation and visible light source. The removal efficiency of SMX was significantly improved when UV light was used due to the higher utilization rate of photons. Although higher rates of antibiotic decomposition can be achieved under UV light [120,121], TiO_2-based photocatalysts have the potential to be efficient enough under solar irradiation [116,118,122] that is a clean and sustainable source of energy [45] and, therefore, is more preferable.

4. Degradation Pathways of Antibiotics

Many researchers have studied degradation pathways of sulfamethoxazole in photocatalytic processes over TiO_2 and TiO_2-based materials, for example, Yuan et al. [84], Gong and Chu [86], Xie et al. [79], Wang et al. [89], Mourid et al. [90], Borowska et al. [123], and Yu et al. [124]. They reported three degradation reactions to be the main transformation pathways: hydroxylation, cleavage of S-N bond and isoxazole ring opening. Although different research groups obtained different amounts and types of photoproducts (from six intermediates over Bi_2O_3-TiO_2/PAC [89] and LDH-TiO_2 [90] to sixteen intermediates over $CoFe_2O_4$/TiO_2 [86]), the main transformation products of SMX ($C_{10}H_{11}N_3O_3S$, *m/z 253*) in the studies are the following: $C_{10}H_{12}N_3O_4S$, *m/z 269;* $C_{10}H_{13}N_3O_5S$, *m/z 287;* $C_8H_9N_3O_4S$, *m/z 243;* $C_6H_7N_3O_2S$, *m/z 197;* $C_6H_7NO_3S$, *m/z 173;* $C_6H_6O_3S$, *m/z 158*; and C_6H_7N, *m/z 93*. Proposed pathways of SMX photocatalytic oxidation are presented in Scheme 2 (products are labeled as P followed by the corresponding mass of the compound). Photoproducts with low molecular weight might be further oxidized to inorganic substances: SO_4^{2-}, NO_3^-, NH^{4+}, H_2O and CO_2 [79,90].

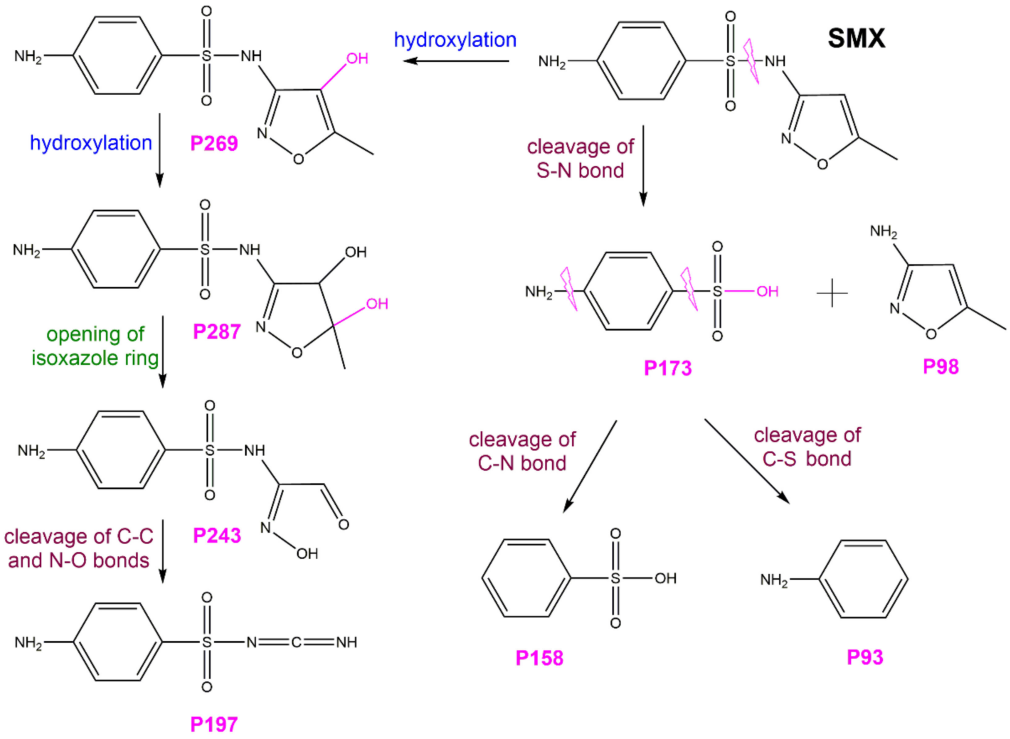

Scheme 2. Proposed degradation pathways of SMX in photocatalytic oxidation over TiO_2.

Photodegradation routes of trimethoprim in TiO_2 photocatalysis are less studied than those of sulfamethoxazole. Sirtori et al. [125] and Samy et al. [126] investigated phototransformation products of TMP when TiO_2 P25 and S-TiO_2 were employed as catalysts, respectively. Both research groups reported hydroxylation, demethylation, and cleavage to be the main transformation pathways in the TMP ($C_{14}H_{18}N_4O_3$; *m/z 291*) degradation process. In the hydroxylation reaction, polyhydroxylated compounds with the general formula of $C_{14}H_{19}N_4O_{3+x}$ (x varying from 1 to 4) are formed. For example, $C_{14}H_{19}N_4O_4$; *m/z 307* and $C_{14}H_{19}N_4O_5$; *m/z 323* occur in this way. In demethylation-hydroxylation reactions, compounds with the general formula of $C_{14-y}H_{19-2y}N_4O_{3+x}$ (y varying from 1 to 3) are formed: $C_{13}H_{17}N_4O_5$, *m/z 309*; $C_{13}H_{17}N_4O_7$, *m/z 341*; $C_{12}H_{15}N_4O_5$, *m/z 295*; $C_{12}H_{15}N_4O_4$, *m/z 279*; $C_{11}H_{13}N_4O_5$, *m/z 281*; and $C_{13}H_{16}N_4O_3$, *m/z 277*. Cleavage of TMP results in the generation of the following products: $C_5H_6N_4O$, *m/z 139*; $C_5H_6N_4O_2$, *m/z 155*; $C_8H_{10}O_4$, *m/z 171*; and $C_5H_8N_4O$, *m/z 141*. Besides, trimethoxybenzoylpyrimidine ($C_{14}H_{17}N_4O_4$, *m/z 305*) is a product of TMP oxidation. Based on the identification of these phototransformation products, a suggestion of possible TMP degradation pathway is presented in Scheme 3 (products are labeled as P followed by the corresponding mass of the compound).

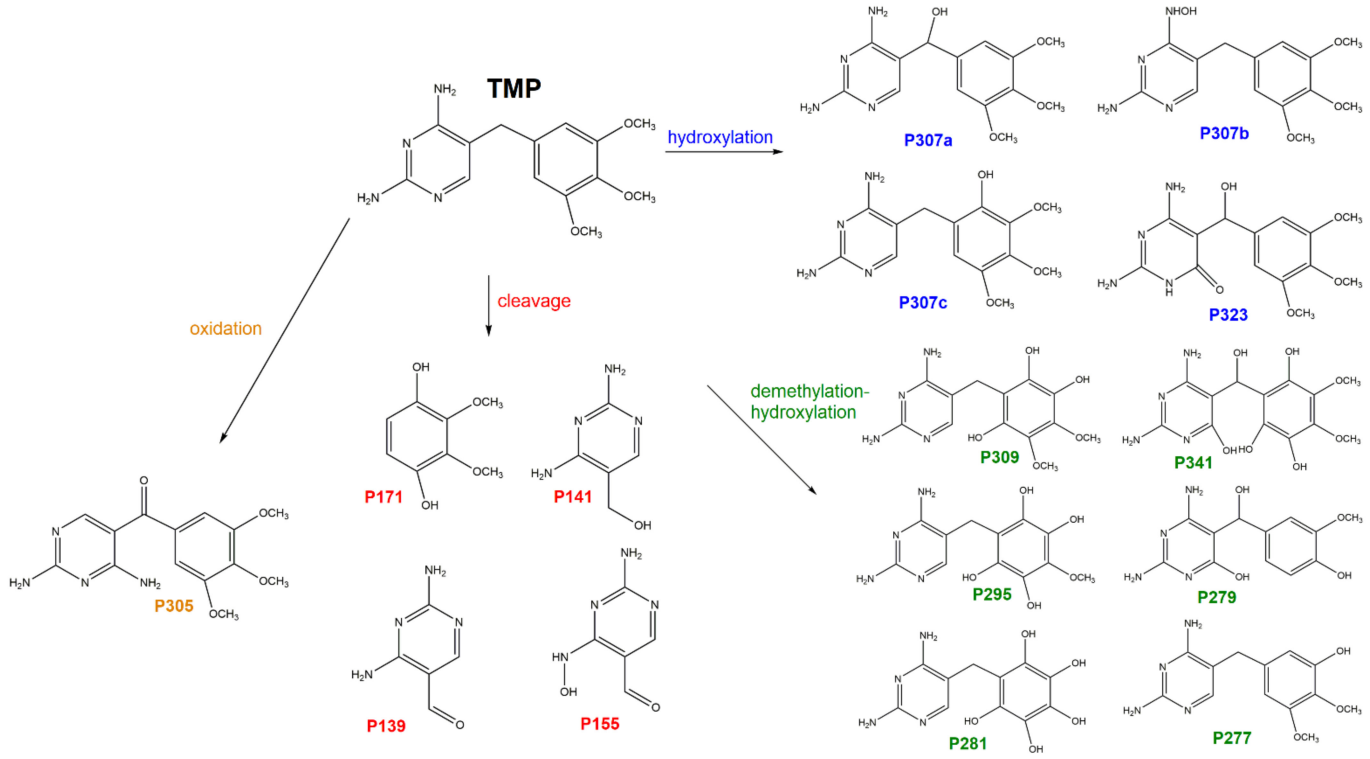

Scheme 3. Proposed degradation pathways of TMP in photocatalytic oxidation over TiO_2.

The photodegradation pathways of ciprofloxacin over TiO_2 and TiO_2-based materials have been studied by many research groups: Wang et al. [114], Sarafraz et al. [24], Manasa et al. [118], Karim and Shriwastav [76], Huerta-Aguilar et al. [109], Li and Hu [96], and Calza et al. [127]. Obtained photoproducts varied greatly and are summarized in an excellent review by Hu et al. [128]. In CIP photodegradation, four main transformation reactions can be outlined: cleavage of piperazine ring, defluorination, decarboxylation and oxidation of the cyclopropyl group. Possible photoproducts in the CIP degradation process are presented in Scheme 4 (products are labeled as P followed by the corresponding mass of the compound).

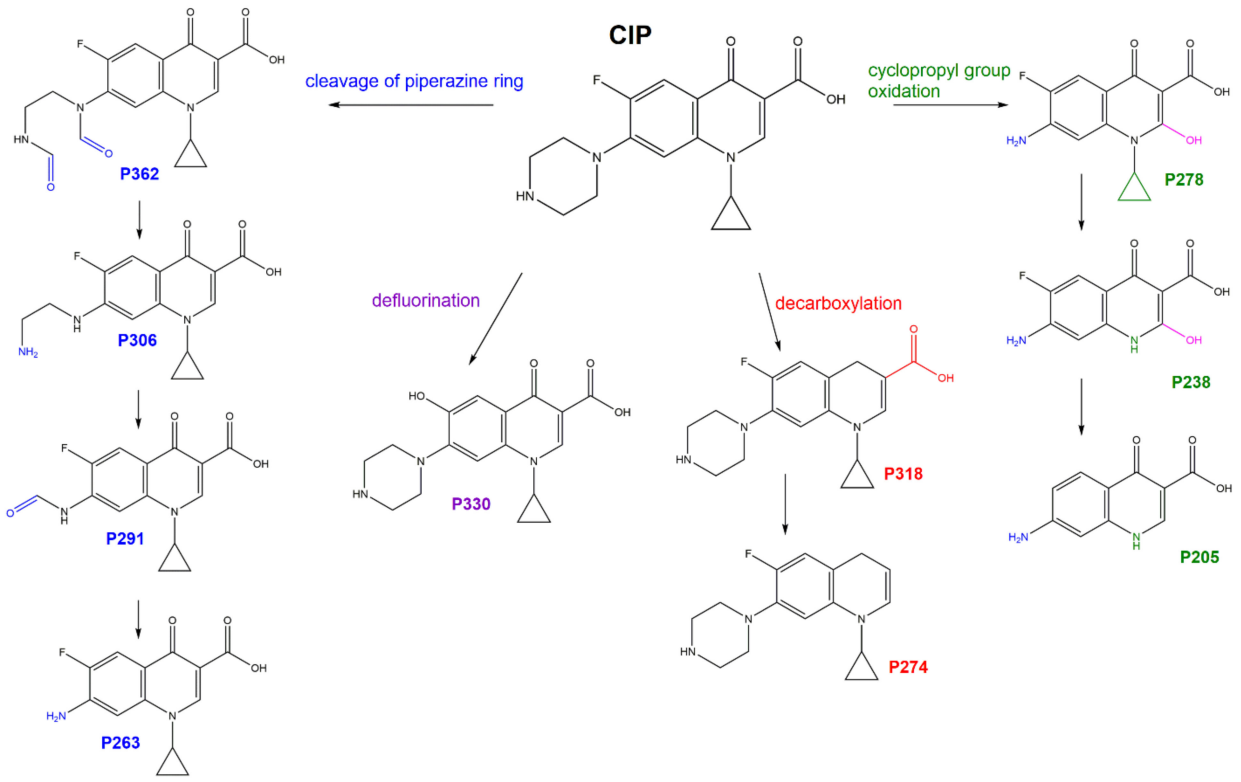

Scheme 4. Proposed degradation pathways of CIP in photocatalytic oxidation over TiO_2.

5. Ecotoxicity of Photoproducts

Considering a wide variety of transformation products occurring during the photocatalytic degradation of antibiotics, evaluation of their toxic effects on ecosystems is highly important for the practical application of the process in water treatment.

The phytotoxicity of photocatalysis products towards plant *Lepidium sativum* was studied by Borowska et al. [123]. After 60 min of solar irradiation of TiO_2 catalysts doped with noble metals, toxicity was eliminated: germination index increased from 43 ± 4% for initial 1 mgL^{-1} SMX solution to 93 ± 10% and 110 ± 16% for solutions treated with Pd/TiO_2 and Pt/TiO_2, respectively. Decreased ecotoxicity was attributed to very low concentrations of remaining antibiotics. Negligible toxicity towards *Vibrio fischeri* and fully removed antibiotic activity against *E. coli* was achieved by Durán-Álvarez et al. [121], when 30 mgL^{-1} CIP solution was treated using TiO_2 modified with bi-metallic nanoparticles. This was a result of the complete mineralization of the parent compound after 360 min of photocatalytic treatment under simulated sunlight irradiation.

The antimicrobial activity of 15 mgL^{-1} CIP solution towards *Vibrio fischeri* was diminished significantly upon a photocatalytic process with graphitized mesoporous carbon-TiO_2 nanocomposite under UV-C irradiation in the study carried out by Zheng et al. [129]. Resulting non-toxicity was attributed to the almost complete mineralization of the antibiotic after 120 min of reaction. Cai and Hu [75] applied UV/TiO_2 P25 system and observed no acute toxicity (30 min of incubation) of 1 ppm SMX and 1 ppm TMP towards *Vibrio fischeri*. However, significant chronic toxicity (24 h of incubation) was reported. Sarafraz et al. [24] treated CIP solutions using a N-TiO_2/visible LED system that resulted in significantly decreased toxicity towards *Daphnia magna* compared to the parent compound. A reduction in antibacterial activity of CIP against *Staphylococcus aureus* was also obtained by Gan et al. [130], who applied synthesized TiO_2 under artificial sunlight.

Gong and Chu [86] also observed a significant reduction of toxic activity against aquatic organisms when a UV-C/$CoFe_2O_4/TiO_2$ system for 100 μM SMX degradation

is utilized. In the case of green alga *Chlorella vulgaris*, SMX was suggested to have been transformed into nutrients (source of carbon and inorganic salts) upon photocatalytic process, favoring algae growth. In contrast, SMX and its photoproducts inhibited the feeding of the brine shrimp *Artemia salina*, demonstrating that although the toxic effect of transformation products was significantly decreased, it was not completely eliminated. High rates of SMX decomposition and mineralization contributed to negligible toxicity towards *Daphnia magna* and *Escherichia coli* in the study carried out by Kim and Kan [81]. Researchers utilized UV-C/biochar/TiO_2 system for the photocatalytic degradation of 10 mgL^{-1} SMX and thus, obtained nontoxic products (nitrates, sulfates and some organic acids) after 6 h of reaction. However, when nitrate and bicarbonate were added into reaction solution, toxicity was highly increased up to 100%, suggesting the cautious application of the given process to the treatment of natural water bodies.

Ioannidou et al. [74] reported a small decrease in antimicrobial activity after photocatalytic treatment with the WO_3-doped TiO_2 P25 catalyst, attributed to the slow mineralization of by-products after 180 min of simulated solar irradiation. Ecotoxic effects of SMX and its transformation products in that case were assessed towards bacterial strains: *Escherichia coli* and *Enterococcus faecalis*. During the oxidation process, toxicity first increased from a 50% population reduction of both *E. coli* and *E. faecalis* (20 mgL^{-1} initial SMX solution) to 64% and 57%, but eventually decreased to 45% and 37%, respectively. Murgolo et al. [131] also observed only a partial decrease in toxicity when a synthesized TiO_2 catalyst was utilized under UV-C irradiation for the photocatalytic degradation of a mixture of pharmaceuticals containing TMP. Acute toxicity tests were performed with green alga *Selenastrum capricornutum*, embryo of fish *Danio rerio* (FET) and AMES fluctuation test.

However, Nasuhoglu et al. [85] observed the formation of more toxic products towards *Daphnia magna* than initial 60 mgL^{-1} SMX solution when the target antibiotic was treated with UV-C/TiO_2 P25 for 13 h. Sirtori et al. [125] also reported the increased inhibition of *Vibrio fischeri* by TMP transformation products compared to parent compound (20 mgL^{-1} TMP), both in demineralized water and seawater, when the photocatalytic process with TiO_2 P25 under solar irradiation was carried out. In addition, the toxicity of CIP solutions treated by UV-A/TiO_2 P25 increased towards *Vibrio fischeri* compared to the original compound in the work of Silva et al. [132]. Although toxicity decreased after 15 min of the photocatalytic process, CIP solutions became very toxic (70% of luminescence inhibition) after 45 min of treatment due to higher quantities of transformation products being generated. An interesting observation was made by Yang et al. [105]: the antimicrobial activity of SMX transformation products against bacteria *Vibrio fischeri* increased compared to the parent compound (50 mgL^{-1} SMX) when photocatalytic tests were carried out in distilled water (UV-A/TiO_2 P25 system, 510 min). However, no significant toxicity was observed when tests were performed in different media: seawater with 20‰ and 34‰ salinity. Explanation for such findings might be in decreased photocatalytic decomposition of antibiotic when salinity was increased. Thus, smaller quantity of transformation products resulted in decreased biotoxicity. Xing et al. [133] utilized Toxicity Estimation Software Tool (T.E.S.T.) software to assess the toxicity of initial CIP solution and its photoproducts. Although most of the transformation products were reported to be less toxic than untreated antibiotic, some degradation products were found to be more toxic.

The photocatalytic performance of various TiO_2 and TiO_2-based materials in degradation processes of sulfamethoxazole, trimethoprim and ciprofloxacin, along with photocatalysts characterization and process description, is presented in Table 4.

Table 4. Performance of various TiO_2 and TiO_2-based materials in photocatalytic degradation of SMX, TMP and CIP.

Catalyst	Characteristics	Process conditions	Performance	Ref.
		Sulfamethoxazole		
Kaolinite Clay-TiO_2-$ZnWO_4$ and agrowaste (*carica papaya* seeds or *musa paradisiaca* peels) nanocomposite	Particle size: 62–257 nm (SEM)Band gap: 2.56–2.89 eV	Medium: Ultrapure water Ant. Conc.: 0.05 gL^{-1} Cat. Conc: 0.05 gL^{-1} pH: 6.8Light source: sunlight irradiation (10 AM–5 PM) Cat.: $TZPP_5$ (based on *musa paradisiaca* peels and calcined at 500 °C)	Photodegradation: 60% (60 min) Mineralization: 50% (60 min) COD k(1st) = 0.0227 min^{-1} $t_{1/2}$ = 30.48 minStability: over 4 cycles	[73]
LDH-TiO_2 (Zn_2-Al-CO_3/TiO_2 P25)	-	Ant. Conc.: 0.02 gL^{-1} Cat. Conc.: 0.5 gL^{-1} pH: 10Light source: 300 W UV-A lamp (300–400 nm) with high pressure tungsten filament Cat.: LDH-TiO_2 (10% TiO_2)	Photodegradation: 100% (360 min) Mineralization: 100% (144 h) COD Stability: 90.5% after 5 cycles	[90]
TiO_2 P25 (Evonik, Germany)	Particle size: 21 nm Composition: 80% anatase, 20% rutile BET surface: 35–65 m^2g^{-1} Band gap: 3.2 eV	Medium: deionized water Ant. Conc.: 0.001 gL^{-1} Cat. Conc.: 0.1 gL^{-1} pH: 6.0 Light source: solar simulation chamber with a 1.5 kW Xenon lamp (290–400 nm) Temperature: 20 °C	Photodegradation: 100% (120 min) k(1st) = 0.041 min^{-1}	[104]
F-Pd co-doped TiO_2	Particle size: 5–25 nm (TEM) Band gap: 0.54–3.26 eV	Medium: deionized water Ant. Conc.: 0.03 gL^{-1} Cat. Conc.: 1 gL^{-1} Light source: direct sunlight irradiation Temperature: 29–31 °C Cat.: FPd-TiO_2 (10 mol.% Pd)	Photodegradation: 98.4% (40 min) Mineralization: 93% (40 min) TOC	[116]
Bi_2O_3-TiO_2/PAC (powdered activated carbon)	Crystallite size: 48 nm (XRD) Band gap: 2.58 eV	Medium: deionized water Ant. Conc.: 0.02 gL^{-1} Cat. Conc.: 0.2 gL^{-1} Light source: solar simulator (300 W Xe arc lamp)	Photodegradation: 100% (30 min) Stability: 90.4% after 5 cycles	[89]
TiO_2 P25	Particle size: 21 nm Composition: 80% anatase, 20% rutile BET surface: ~50 m^2g^{-1} Band gap: 3.2 eV	Ant. Conc.: 0.04 gL^{-1} Cat. Conc.: 0.024 gL^{-1} pH: 6.0 Light source: UV-C (254 nm), light intensity 15 mW cm^{-2}Temperature: 25 °C	Photodegradation: 95.0% (120 min) Mineralization: 66% (120 min) TOC	[84]
TiO_2	BET surface: 52 m^2 g^{-1}Band gap: 3.08 eV	Ant. Conc.: 100 μgL^{-1} Cat. Conc.: 0.2 gL^{-1} Light source: solar simulator with Xenon lamp (UV irradiance 30 Wm^{-2})	Photodegradation: 100% (30 min)	[134]
Au-TNWs/TNAs (Au nanoparticle-decorated TiO_2 nanowires on TiO_2 nanotube arrays)	Composition: 100% anatase Crystallite size: 21.3–24.7 nm (XRD)	Medium: blank wastewater samples with 0.1% (v.v) formic acid Ant. Conc.: 500 ng/mL, 30mL solutions Light source: UV-VIS 100 W Xenon lamp, 120 $mWcm^{-2}$ Temperature: 32–33 °C	Photodegradation: k(1st) = 1.05 min^{-1}	[135]

Table 4. *Cont.*

Catalyst	Characteristics	Process conditions	Performance	Ref.
Fe/TiO_2	Composition: 100% anatase Crystallite size: 27 nm (XRD) Band gap: 3 eV	Medium: ultrapure water Ant. Conc.: 234 μgL^{-1} Cat. Conc.: 1 gL^{-1} pH: 6 Light source: solar simulator with 100 W Xenon lamp Cat.: 0.04 mol.% Fe	Photodegradation: 95% (90 min) k(1st) = 0.029 min^{-1} Stability: 5 cycles (55%)	[136]
TiO_2	Composition: 93% anatase, 7% rutile Crystallite size: 8.91 nm anatase; 14.7 nm rutile (XRD) BET surface: 134 m^2g^{-1}	Medium: ultrapure water Ant. Conc.: 0.03 gL^{-1} Cat. Conc.: 0.5 gL^{-1} pH: 5.1 Light source: medium pressure mercury vapour lamp (UV-vis: $\lambda > 350$ nm; 50 $mWcm^{-2}$)	Photodegradation: 100% (120 min) Mineralization: 40% (180 min) TOC	[137]
TiO_2/CNT (carbon nanotubes), 10% CNT	Composition: 97% anatase, 3% rutile Crystallite size: 14.6 nm anatase; 40.7 nm rutile (XRD) BET surface: 142 m^2g^{-1}		Photodegradation: 100% (120 min) Mineralization: 70% (180 min) TOC Stability: 3 cycles	
Pt/TiO_2 P25 (1.0 wt.% Pt)	Composition: 80% anatase, 20% rutile Crystallite size: 220 nm anatase, 216 nm rutile (XRD) BET surface: ~50 m^2g^{-1} Band gap: 3.18 eV	Medium: ultrapure water Ant. Conc.: 0.001 gL^{-1} Cat. Conc.: 0.05 gL^{-1} Light source: natural sunlight	Photodegradation: 90% (30 min) k(1st) = 0.076 min^{-1} $t_{1/2}$ = 9.1 min Mineralization: 29±10% (60 min) DOC, C_{cat} = ~25 mgL^{-1} Ecotoxicity: *Lepidium sativum*, no phytotoxicity	[123]
Pd/TiO_2 P25 (1.0 wt.% Pd)	Composition: 89% anatase, 11% rutile Crystallite size: 206 nm anatase, 180 nm rutile (XRD) BET surface: ~50 m^2g^{-1} Band gap: 2.92 eV		Photodegradation: 100% (10 min) k(1st) = 0.521 min^{-1} $t_{1/2}$ =1.3 min Mineralization: 45 ± 2% (60 min) DOC, C_{cat} = ~25 mgL^{-1} Ecotoxicity: *Lepidium sativum*, no phytotoxicity	
$Ce_{0.8}Gd_{0.2}O_{2-\delta}/TiO_2$	Particle size: 7–20 nm (TEM) Composition: 55.78% ceria; 27.01% rutile; 17.21% anatase Crystallite size: 72.94 nm TiO_2; 19.71 nm $Ce_{0.8}Gd_{0.2}O_{2-\delta}$ (XRD) BET surface: 5.11 m^2g^{-1} Band gap: 2.84 eV	Ant. Conc.: 0.025 gL^{-1} Cat. Conc.: 0.1 gL^{-1} Light source: 15 W mercury UV lamp	Photodegradation: 97% (120 min) k(2nd) = 0.2959 $mg^{-1}min^{-1}$Stability: 5 cycles	[92]

Table 4. *Cont.*

Catalyst	Characteristics	Process conditions	Performance	Ref.
Biobased-PET-TiO_2 P25 composite films	TiO_2 P25:Particle size: 20–30 nm Composition: 80% anatase; 20% rutile BET surface: 56 m^2g^{-1} PZC: 6.3–6.8	Medium: ultrapure water Ant. Conc.: 0.001 gL^{-1} (for each antibiotic, mixture of eight) Cat. Conc.: 0.05 gL^{-1} Light source: solar simulator with xenon lamp (1.5 kW, 500 Wm^{-2}) Cat.: PET-10%-TiO_2 (10 wt.% of TiO_2)	Photodegradation: 98% (6 h) k(1st) = 0.015 min^{-1} $t_{1/2}$ = 46.2 min Stability: 5 cycles	[103]
Zn-TiO_2/pBC (reed straw biochar)	Crystallite size: 9.4 nm (XRD) BET surface: 169.12 m^2g^{-1}	Medium: ultrapure water Ant. Conc.: 0.01 gL^{-1} Cat. Conc.: 1.25 gL^{-1} pH: 4Light source: 50 W Xenon lamp with 420 nm cutoff filter (visible) Temperature: 25 °C Cat.: Zn10-TiO_2/pBC (10 wt.% Zn)	Photodegradation: 80.81% (3 h) k(1st) = 0.0085 min^{-1} $t_{1/2}$ = 81 min Mineralization: 56.13% (3 h) COD Stability: 5 cycles (77.41%)	[79]
Magnetic carbon nanotube-TiO_2 P25 (MCNT-TiO_2) composites	BET surface: 151 m^2g^{-1}	Medium: ultrapure water Ant. Conc.: 150 μgL^{-1} Cat. Conc.: 0.1 gL^{-1} pH: 7.0±0.2 Light source: solar simulator, 1000 Wm^{-2} Temperature: 26±3 °C Cat.: MCNT-TiO_2 (1:5 mass ratio)	Photodegradation: 92% (30 min) k(1st) = 0.05 min^{-1} Stability: 5 cycles	[101]
TiO_2 P25	Composition: 80% anatase, 20% rutile	Medium: secondary urban wastewater Ant. Conc.: 100 μgL^{-1} Cat. Conc.: 1 gL^{-1} Light source: four 9 W UVA-LEDs, 381 nm	Photodegradation: 100% SMX (30 min) k(1st) = 0.2126 min^{-1} Disinfection: total heterotrophs, E. coli and enterococci	[111]
Porous titanium-titanium dioxide (PTT) substrates	Composition: anatase Band gap: 3.0 eV Isoelectric point: 6.0	Medium: ultrapure water Ant. Conc.: 300 mL of 2 μgL^{-1} (eighteen pharmaceuticals) pH: ~5 Light source: UV-LEDs, 1.7×10^{-3} W, 365 nm	Photodegradation: 72.74% (300 min) k(1st) = 0.00435 min^{-1}	[138]
Graphene-based TiO_2 P25 (TiO_2-rGO)	BET surface: 44.761 m^2g^{-1}	Medium: membrane bioreactor-treated urban wastewater Ant. Conc.: 100 μgL^{-1} (three compounds) Cat. Conc.: 0.1 gL^{-1} pH: 5.2–6.2 Light source: solar simulator with 1 kW Xenon lamp, 63 Wm^{-2}Temperature: 25 ± 1 °C Cat.: TiO_2-rGO-PH	Photodegradation: 50 ± 3% (60 min) Disinfection: *E. coli* complete inactivation (180 min)	[139]
Ag^0(NP)/TiO_2 thin films	Particle size: 10–15 nm (TEM) BET surface: 12.02 m^2g^{-1}	Medium: purified water Ant. Conc.: 50 mL of 1.0 mgL^{-1} pH: 6.0 Light source: 9 W UVA 360 nm Temperature: 25 ± 1 °C Cat.: Ag^0(NP)/TiO_2 (B)	Photodegradation: 57% (120 min) k(1st) = 0.0067 min^{-1} Mineralization: 30.2% (120 min) NPOC Stability: 6 cycles	[72]

Table 4. *Cont.*

Catalyst	Characteristics	Process conditions	Performance	Ref.
TiO_2 supported on reed straw biochar TiO2/pBC	Composition: 100% anatase Crystallite size: 10.1 nm BET surface: 102.16 m^2g^{-1}	Medium: ultrapure water Ant. Conc.: 0.01 gL^{-1} Cat. Conc.: 1.25 gL^{-1} pH: 4.0 Light source: 50 W xenon lamp with visible light filter Temperature: 25 °C Cat.: TiO_2/pBC (300)	Photodegradation: 91.27% (3 h) k(1st) = 0.0130 min^{-1} $t_{1/2}$ = 53.32 minMineralization: 57.44% (3 h) CODStability: 5 cycles	[80]
TiO_2 P25-WO_3	Composition: 77% anatase, 23% rutile Crystallite size: 25 nm anatase, 78 nm rutile (XRD) BET surface: 32 m^2g^{-1} Band gap: 3.0 eV	Medium: ultrapure water Ant. Conc.: 350 μgL^{-1} Cat. Conc.: 0.250 gL^{-1} Light source: solar simulator with 100 W xenon lamp, 420 nm cut-off filter Temperature: 25 °C Cat.: 4% W-P25(700)	Photodegradation: 100% (60 min) solar irradiation 25% (120 min) visible light k(1st) = 0.133 min^{-1} Mineralization: 28% (6 h), 20 mgL^{-1} SMX with 1 gL^{-1} 4% W-P25(700) Ecotoxicity: *Escherichia coli, Enterococcus faecalis*	[74]
TiO_2 P25-Fe immobilized on optical fibers	Grain size: 7.41 nm (XRD)Composition: 54% anatase, 46% rutile Band gap: 2.40 eV	Medium: deionized water Ant. Conc.: 0.005 gL^{-1} Cat. Dosage: 30 pieces of 10 cm photocatalyst-coated SOFs pH: 6.0 Light source: visible light source (halogen lamp 150 W) Temperature: 23 °C	Photodegradation: 35% (6 h) k(1st) = 0.082 min^{-1}	[120]
TiO_2 P25-reduced graphene oxide (TiO2-rGO) immobilized on optical fibers	Grain size: 6.52 nm (XRD)Composition: 69% anatase, 31% rutile Band gap: 2.85 eV		Photodegradation: 35% (6 h) k(1st) = 0.079 min^{-1}	
$CoFe_2O_4/TiO_2$ (+TiO_2 P25)	-	Medium: ultrapure water Ant. Conc.: 100 µM Cat. Conc.: 0.5 gL^{-1} Light source: photo-chemical reactor with twelve mercury lamps (350 nm)	Photodegradation: 100% (5 h) Mineralization: 50% (5 h) TOC Ecotoxicity: green alga *Chlorella vulgaris*, brine shrimp *Artemia salina*	[86]
Biochar/TiO_2	Composition: anatase	Medium: pure water Ant. Conc.: 0.01 gL^{-1} Cat. Conc.: 5 gL^{-1} pH: 4.0 Light source: UV-C, 15 W, 254 nm Temperature: 293 K	Photodegradation: 75% (3 h) Mineralization: 65% (3 h) COD Ecotoxicity: *Daphnia magna, E.Coli*	[81]
TiO_2 (TiEt-450)	Hydrodynamic particle size: 3.0 µm Composition: 100% anatase BET surface: 43 m^2g^{-1} Isoelectric point: 7.1 Band gap: 3.22 eV	Medium: deionized water Ant. Conc.: 100 μgL^{-1} of each contaminant (mixture of five, 500 μgL^{-1} in total) Cat. Conc.: 0.5 gL^{-1} pH: natural Light source: solar radiation pilot plant Temperature: ambient	Photodegradation: 100% (30 min) k(1st) = 0.095 min^{-1}	[102]

Table 4. *Cont.*

Catalyst	Characteristics	Process conditions	Performance	Ref.
TiO_2 P25	Particle size: 30 nm Composition: 70% anatase, 30% rutile BET surface: 50 ± 15 m^2g^{-1} Band gap: 3.15 eV	Medium: high purity water Ant. Conc.: 0.02 gL^{-1} Cat. Conc.: 0.5 gL^{-1} pH: natural Light source: UV-LEDs: 365 ± 10 nm, 300 ± 5 nm, and 260 ± 10 nm Temperature: 25 °C	Photodegradation: 58% (3 h) UV-A 85% (3 h) UV-B 100% (3 h) UV-C Mineralization:35.1% (3 h) UV-A 40.5% (3 h) UV-B 59.9% (3 h) UV-C	[119]
TiO_2 immobilized on porous supports: quartz fiber filters (QFT) or porous titanium sheets (PTT)	Composition: anatase Isoelectric point: 4 (QFT), 6 (PTT) Band gap: 3.18 eV (QFT), 3.0 eV (PTT)	Medium: ultrapure water Ant. Conc.: 300 mL of 2.0 μgL^{-1} pH: 4.5–5 Light source: UV-LED 365 nm, 1.7 mW, 0.13 mW/cm^2 Temperature: 24 ± 2 °C Cat.: TiO_2 PTT	Photodegradation: k(1st) = 0.0069 min^{-1} Stability: 2 cycles	[140]
TiO_2 P25 immobilized on PVDF-coated steel mesh (SM-TiO_2)	-	Ant. Conc.: 10 μM Cat. Conc.: 0.02 gL^{-1} pH: 6.8–7.0 Light source: six blacklight blue lamps, 4 W, 350–400 nm	Photodegradation: 100% (120 min) k(1st) = 0.0568 min^{-1} Mineralization: 15% (180 min) TOC Stability: 20 cycles	[141]
Floating TiO_2-expanded perlite (EP-TiO_2-773)	-	Medium: deionized water Ant. Conc.: 0.1 gL^{-1} Cat. Conc.: 3.33 gL^{-1} pH: 10 Light source: photoreactor with six (8 W each) lamps, 316–400 nm	Photodegradation: k(0st) = 4.57×10^{-6} min^{-1}	[91]
Nano-sized TiO_2 supported on single wall carbon nanotubes (SWCNTs/TiO_2)	Composition: anatase	Medium: ultrapure water Ant. Conc.: 200–500 μgL^{-1} Cat. Conc.: 0.1 gL^{-1} Light source: low pressure mercury lamp, 17 W, 254 nm, 0.1 Wcm^{-2}	Photodegradation: k(1st) = 0.42 min^{-1} Stability: 5 cycles	[142]
Cu–TiO_2 P25	Particle size: 21 ± 4 nm (TEM) BET surface: 52–59 m^2g^{-1}	Medium: oxygen-saturated waterAnt. Conc.: 0.004 gL^{-1} Cat. Conc.: 1 gL^{-1} pH: 5.2 Light source: eight 8 W lamps, 77 $mWcm^{-2}$, 460 nm visible light Cat.: Cu–TiO_2 P25 (0.045 wt.% Cu)	Photodegradation: 100% (90 min) k(1st) = 0.0506 min^{-1} Stability: 4 cycles	[82]
TiO_2 P25	Particle size: 21 nm	Medium: distilled water Ant. Conc.: 0.05 gL^{-1} Cat. Conc.: 0.1 gL^{-1} Light source: UVA 15 W, 360 nm, 1.15 $mWcm^{-2}$ Temperature: 25 ± 2 °C	Photodegradation: 92.3% (510 min) $t_{1/2}$ = 132 ± 5 min Mineralization: 34% (510 min) CODEcotoxicity: *Vibrio fischeri*	[105]
TiO_2 P25	-	Medium: purified water Ant. Conc.: 400 ppb each (mixture of two antibiotics) Cat. Conc.: 0.05 gL^{-1} pH: 5.6 Light source: thirty two 1W UVA/LED chips, peak emission at 365 nm Temperature: 25 °C	Photodegradation: 91% (20 min) Disinfection: *Escherichia coli* Ecotoxicity: *Vibrio fischeri*	[75]

Table 4. *Cont.*

Catalyst	Characteristics	Process conditions	Performance	Ref.
		Trimethoprim		
TiO_2 P25	-	Medium: purified water Ant. Conc.: 400 ppb each (mixture of two antibiotics) Cat. Conc.: 0.05 gL^{-1} pH: 5.6 Light source: thirty two 1W UVA/LED chips, peak emission at 365 nm Temperature: 25 °C	Photodegradation: 96% (20 min) Disinfection: *Escherichia coli* Ecotoxicity: *Vibrio fischeri*	[75]
Biobased-PET-TiO_2 P25 composite films	TiO_2 P25: Particle size: 20–30 nm Composition: 80% anatase; 20% rutile BET surface: 56 m^2g^{-1} ZPC: 6.3–6.8	Medium: ultrapure water Ant. Conc.: 0.001 gL^{-1} (for each antibiotic, mixture of eight) Cat. Conc.: 0.05 gL^{-1} Light source: solar simulator with xenon lamp (1.5 kW, 500 Wm^{-2}) Cat.: PET-10%-TiO_2 (10 wt.% of TiO_2)	Photodegradation: 90% (6 h) k(1st) = 0.007 min^{-1} $t_{1/2}$ = 99.0 min Stability: 5 cycles	[103]
Keratin-TiO_2 nanocomposite	Composition: 85% anatase; 15% rutile	Ant. Conc.: 0.172 mM Cat. Conc.: 1 gL^{-1} Light source: Xenon lamp, simulated solar light, 28 kLux Temperature: 25 °C Cat.: K-TiO_2 10%	Photodegradation: 100% (4 h) Stability: 4 cycles	[143]
S-TiO_2	Particle size: 12–22 nm (TEM) Composition: anatase; brookite	Ant. Conc.: 0.01 gL^{-1} Cat. Conc.: 0.5 gL^{-1} pH: 7.0 Light source: UV-Vis 400 W metal halide lamp	Photodegradation: 98.2% (4 h) Stability: 5 cycles (for immobilized catalyst)	[126]
TiO_2 P25	Composition: 80% anatase, 20% rutile	Medium: secondary urban wastewater Ant. Conc.: 100 μgL^{-1} Cat. Conc.: 1 gL^{-1} Light source: 4 UVA-LEDs, 9 W, 381 nm	Photodegradation: 100% (60 min) k(1st) = 0.1171 min^{-1} Disinfection: total heterotrophs, *E. coli* and *enterococci*	[111]
Nitrogen-doped TiO_2 immobilized on polystyrene spheres (N-TiO_2)	Composition: anatase Band gap: 2.5 eV	Medium: distilled water Ant. Conc.: 200 μgL^{-1} Cat. Conc.: 160.74 gL^{-1} pH: 6.13–6.38 (not adjusted) Light source: natural sunlight Temperature: 25.7–36.1 °C (not adjusted)	Photodegradation: 100% (150 min) k(1st) = 0.0167 min^{-1} $t_{1/2}$ = 42 min	[117]
Porous titanium-titanium dioxide (PTT) substrates	Composition: anatase Band gap: 3.0 eV Isoelectric point: 6.0	Medium: ultrapure water Ant. Conc.: 300 mL of 2 μgL^{-1} (eighteen pharmaceuticals) pH: ~5 Light source: UV-LEDs, 1.7×10^{-3} W, 365 nm	Photodegradation: 31.78% (300 min) k(1st) = 0.00132 min^{-1}	[138]
Nano-sized TiO_2 supported on single wall carbon nanotubes (SWCNTs/TiO_2)	Composition: anatase	Medium: ultrapure water Ant. Conc.: 200–500 μgL^{-1} Cat. Conc.: 0.1 gL^{-1} Light source: low pressure mercury lamp, 17 W, 254 nm, 0.1 Wcm^{-2}	Photodegradation: k(1st) = 0.075 min^{-1} Stability: 5 cycles	[142]

Table 4. *Cont.*

Catalyst	Characteristics	Process conditions	Performance	Ref.
Immobilized TiO_2 P25 on poly(vinylidene fluoride) (PVDF) dual layer hollow fibre membrane	Composition: anatase, rutile BET surface: 50 m^2g^{-1}	Medium: ground water and secondary wastewater effluent Ant. Conc.: 200–400 μgL^{-1} Cat. Conc.: 0.057 gL^{-1} Light source: low-pressure mercury UV lamp, 40 W, 254 nm	Photodegradation: k(1st) = 0.045 min^{-1} (ground water) k(1st) = 0.095 min^{-1} (secondary WW effluent)Stability: 5 cycles	[144]
TiO_2 film deposited on stainless steel mesh (nanoTiO_2-SS)	-	Medium: filtered ground water Ant. Conc.: 200–400 μgL^{-1} Cat. Conc.: 0.1 gL^{-1} pH: 7.85 Light source: 40 W Hg low pressure UV lamp, 254 nm, 50 $mWcm^{-2}$ Temperature: 24.8 °C	Photodegradation: k(1st) = 0.107 min^{-1} Ecotoxicity: AMES Fluctuation, Fish Embryo, Green alga *Selenastrum capricornutum, Daphnia magna. Vibrio fischeri* Stability: 10 cycles	[131]
Ciprofloxacin				
Black Ti^{3+}/N-TiO_2 P25 (b-N-TiO_2)	Particle size: < 100 nm (FE-SEM) Composition: anatase BET surface: 100 m^2g^{-1} PZC: 7.9 Band gap: 2.0 eV	Medium: ultrapure water Ant. Conc.: 0.5 mgL^{-1} Cat. Conc.: 0.43 gL^{-1} pH: 6.7 Light source: 5 W visible LED lamp, 550 nm	Photodegradation: 100% (70 min) k(1st) = 0.0778 min^{-1} Mineralization: 82% (140 min) TOC Ecotoxicity: *Daphnia magna* Stability: 5 cycles	[24]
3D tripyramid TiO_2 architectures	Particle size: 10 nm (TEM) Composition: anatase BET surface: 84 m^2g^{-1} Band gap: 3.2 eV	Ant. Conc.: 32.6 µM Cat. Conc.: 0.1 gL^{-1} Light source: UV-vis light	Photodegradation: 90% (60 min) k(1st) = 0.0403 min^{-1} Stability: 5 cycles	[97]
TiO_2 nanorod/g-C_3N_4 nanosheet (TiO_2 nanorod-CN)	Composition: anatase ZPC: 6.3 Band gap: 2.95 eV	Ant. Conc.: 15 $\mu molL^{-1}$ Cat. Conc.: 0.2 gL^{-1} pH: 6.3 Light source: simulated sunlight irradiation, 500 W Xenon lamp Cat.: 30 wt.% g-C_3N_4	Photodegradation: 93.4% (60 min) k(1st) = 0.0389 min^{-1}	[94]
TiO_2-Ag NPs	Particle size: 80–100 nm (SEM)Composition: >90% anatase, rutile (XRD) Grain size: 51.56 nm anatase, 21.87 nm rutile (XRD) Band gap: 3.26–3.30 eV	Ant. Conc.: 1.0 mM Cat. Conc.: 0.001 gL^{-1} pH: 7.0 Light source: 120 W UV Hg lamp; natural sunlight	Photodegradation: 85.21% UV light k = 1.53 mMs^{-1} 75.58% visible light k = 1.20 mMs^{-1}	[109]
TiO_2 P25 (Acros) and γ-Fe_2O_3 co-doped graphene oxide (GO) nanosheets(TiO_2/γ-Fe_2O_3/GO)	Composition: anatase, rutile Band gap: 2.43 eV	Ant. Conc.: 0.01 gL^{-1} Cat. Conc.: 0.4 gL^{-1} pH: 6.6 Light source: 300 W xenon lamp, 420 nm cutoff filter Cat.: 0.03TiO_2/γ-Fe_2O_3/GO	Photodegradation: 99% (140 min) k(1st) = 0.019 min^{-1} Stability: 4 cycles	[114]

Table 4. *Cont.*

Catalyst	Characteristics	Process conditions	Performance	Ref.
TiO_2/kaolinite	Crystallite size: 16.631 nm (XRD) Composition: anatase BET surface: 60.21 m^2g^{-1} Band gap: 3.18 eV	Medium: deionized water Ant. Conc.: 20 ppm Cat. Conc.: 2 gL^{-1} Light source: high-pressure mercury lamp Cat.: TK-6.0 (58.54% TiO_2)	Photodegradation: 93.14% (40 min) k(1st) = 0.04549 min^{-1} Stability: 4 cycles	[145]
Fe–N–TiO_2	Particle size: ~25 nm (HR-TEM) Composition: 61.1% anatase, 21.4% rutile, 17.5% brookite Crystallite size: 28.1 nm anatase, 28.7 nm rutile, 34.3 nm brookite (XRD) BET surface: 90.2 m^2g^{-1} Band gap: 2.7 eV	Ant. Conc.: 0.02 gL^{-1} Cat. Conc.: 1 gL^{-1} Light source: 12 W LED daylight lamps (visible) Temperature: ambient Cat.: 2.5%N–1.5%Fe	Photodegradation: 67.72% (6 h) k(1st) = 0.00552 min^{-1} Mineralization: 49.07% (6 h) TOC	[146]
N-TiO_2	Particle size: 15 ± 0.56 nm (TEM) Composition: anatase, rutile Crystallite size: 12–18 nm (XRD) BET surface: 24.59 m^2g^{-1} PZC: 5.76 Band gap: 2.84 eV	Medium: distilled water Ant. Conc.: 0.01 gL^{-1} Cat. Conc.: 0.5 gL^{-1} pH: 7.0 Light source: three 14 W blue LEDs, 457 nm Cat.: Ti:N molar ratio 1:1	Photodegradation: 55% (180 min) Mineralization: 24% (180 min) TOC	[76]
B-TiO_2 P25	Particle size: 61.8 nm (nanoparticle size analyzer) 25–34 nm (TEM) Composition: anatase, rutile Crystallite size: 19.82 nm anatase, 26.24 nm rutile (XRD) BET surface: 30.1 m^2g^{-1} Band gap: 2.89 eV	Ant. Conc.: 0.01 gL^{-1} Cat. Conc.: 1 gL^{-1} pH: 7.0 Light source: natural sunlight Temperature: 33 °C Cat.: 1B-TiO_2 (1 at.% B)	Photodegradation: 93.16% (180 min) k(1st) = 0.0249 min^{-1} Mineralization: 93% (180 min) COD Disinfection: 95–99.99% efficiency against *E.coli* Stability: 3 cycles	[118]
Ce-TiO_2 P25	Particle size: 89.5 nm (nanoparticle size analyzer), 19–39 nm (TEM)Composition: anatase, rutile Crystallite size: 16.95 nm anatase, 23.21 nm rutile (XRD) BET surface: 41.5 m^2g^{-1} Band gap: 2.50 eV	Ant. Conc.: 0.01gL^{-1} Cat. Conc.: 0.5 gL^{-1} pH: 7.0 Light source: natural sunlight Temperature: 33 °C Cat.: 1Ce-TiO_2 (1 at.% Ce)	Photodegradation: 93.22% (180 min) k(1st) = 0.0266 min^{-1} Mineralization: 92% (180 min) COD Disinfection: 95–99.99% efficiency against *E.coli* Stability: 3 cycles	[118]
Graphene/TiO_2/g–C_3N_4 (GTOCN)	Particle size: 227.18 nm BET surface: 26.41 m^2g^{-1} PZC: 4.16	Medium: ultrapure water Ant. Conc.: 0.003 gL^{-1} Cat. Conc.: 0.6 gL^{-1} Light source: 300 W Xenon lamp (>400 nm), 300 $mWcm^{-2}$ Cat.: GTOCN3 (40 mg Ti_3C_2)	Photodegradation: 61.7% (60 min) k(1st) = 0.01675 min^{-1} Mineralization: 41.8% (60 min) TOC Stability: 3 cycles	[77]

Table 4. *Cont.*

Catalyst	Characteristics	Process conditions	Performance	Ref.
TiO_2 nanotube arrays (TiO_2 NTAs) with Ag_3PO_4 nanoparticles	Composition: anatase BET surface: 4.7 m^2g^{-1} Band gap: < 3.25 eV	Ant. Conc.: 0.01 gL^{-1} Cat. Conc.: 1 gL^{-1} Light source: 300 W Xenon lamp, visible light, 200 $mWcm^{-2}$Cat.: 0.6Ag_3PO_4/TiO_2 (Ag_3PO_4:TiO_2 mass ratio 0.6:1)	Photodegradation: 85.3% (60 min) k(1st) = 0.02499 min^{-1} Disinfection: *E. coli* 100% (120 min) Stability: 3 cycles	[99]
Nitrogen and carbon co-doped TiO_2 nano-catalysts (NCD-TiO_2)	Particle size: 9 nm (HR-TEM) Composition: anatase Crystallite size: 8.8 nm (XRD) BET surface: 116.5 m^2g^{-1} Band gap: 2.94 eV	Medium: ultrapure water Ant. Conc.: 75 µM Cat. Conc.: 1 gL^{-1} pH: 5.7 Light source: four 8 W fluorescent lamps with UV light filter, 11.58 $mWcm^{-2}$ Cat.: NCD200-430 (N:Ti molar ratio 2:1 calcined at 430 °C)	Photodegradation: 68.7% (120 min) k(1st) = 0.0093 min^{-1}	[98]
TiO_2/Graphene oxide	Composition: anatase Crystallite size: 12.5 nm (XRD) BET surface: 91.25 m^2g^{-1} Band gap: 2.47 eV	Medium: distilled water Ant. Conc.: 0.005 gL^{-1} Cat. Conc.: 0.5 gL^{-1} Light source: visible light Cat.: TiO_2/GO (8%)	Photodegradation: 96.73% (60 min) Stability: 6 cycles	[108]
$TiOF_2$/TiO_2 nanosheets	Composition: anatase Crystallite size: 26.2 nm (XRD) BET surface: 119 m^2g^{-1} Band gap: 3.285 eV	Ant. Conc.: 0.02 gL^{-1} Cat. Conc.: 1 gL^{-1} Light source: 300 W Xenon lamp (UV+visible) Cat.: S-160 (hydrothermal treatment at 160 °C)	Photodegradation: 95.3% (90 min) k(1st) = 0.034 min^{-1}	[147]
Cu-TiO_2	Particle size: 10 nm Cu (TEM) 200–400 nm Cu (SEM) Composition: anatase BET surface: 170.15 m^2g^{-1} Band gap: 3.0 eV	Medium: deionized water Ant. Conc.: 0.08 gL^{-1} Cat. Conc.: 0.25 gL^{-1} Light source: 500 W Xenon lamp (simulated sunlight) Cat.: 0.1-Cu-TiO_2 (weight ratio of Cu)	Photodegradation: 97% (4 h) k(1st) = 0.63 min^{-1}Stability: 6 cycles	[100]
Ag-$SrTiO_3$/TiO_2 ($SrTiO_3$ nanocubes supported on TiO_2 nanosheets with Ag nanoparticles deposited on both)	Particle size: 30 nm Ag (SEM) Composition: anatase BET surface: 28.3 m^2g^{-1}	Ant. Conc.: 0.02 gL^{-1} Cat. Conc.: 0.4 gL^{-1} Light source: 300 W Xenon lamp (simulated sunlight)	Photodegradation: 97.6% (60 min) k(1st) = 0.07 min^{-1}	[115]
TiO_2-modified Bi_2MoO_6 nanocrystals TiO_2/Bi_2MoO_6	Particle size: 20 nm Bi_2MoO_6, 12.4 nm rutile, 6.1 nm diameter and 19.1 nm length rod-like anatase (TEM) Composition: Bi_2MoO_6, rutile, anatase BET surface: 17.7 m^2g^{-1} Band gap: 2.60–2.68 eV	Ant. Conc.: 0.01 gL^{-1} Cat. Conc.: 0.6 gL^{-1} Light source: 350 W Xenon lamp, $\lambda \geq$ 420 nm Cat.: TiO_2(0.41 wt%)/Bi_2MoO_6	Photodegradation: 88% (150 min) k(1st) = 0.008 min^{-1}	[148]

Table 4. *Cont.*

Catalyst	Characteristics	Process conditions	Performance	Ref.
N–TiO_2	Particle size: 180 nm length and 50 nm width (FIB/FESEM) Composition: anatase BET surface: 42.70 m^2g^{-1} Band gap: 3.17 eV	Medium: deionized water Ant. Conc.: 20 ppm Cat. Conc.: 1 gL^{-1} pH: 5.5 Light source: three 20 W UV-A lamps 365 nm, 0.493 $mWcm^{-2}$ Cat.: 12.5% N	Photodegradation: 94.29% (420 min) Mineralization: 66.31% (420 min) TOC	[149]
Graphitized mesoporous carbon (GMC)-TiO_2	Particle size: 15 nm (TEM)Composition: anatase Crystallite size: 12 nm (XRD) BET surface: 286 m^2g^{-1}	Medium: deionized water Ant. Conc.: 0.015 gL^{-1} Cat. Conc.: 0.35 gL^{-1} Light source: 14 W UV lamp, 254 nm	Photodegradation: 100% (90 min) k(1st) = 0.102 min^{-1} Mineralization: 100% (120 min) TOC Ecotoxicity: *Vibrio fischeri*	[129]
Mesoporous nano-TiO_2	Composition: anatase Crystallite size: 13.5 nm (XRD) BET surface: 191.4 m^2g^{-1} Band gap: 2.95 eV	Medium: deionized water Ant. Conc.: 0.16 gL^{-1} Cat. Conc.: 0.25 gL^{-1} Light source: 500 W Xe lamp, 200–1000 nm Cat.: TiO_2 (hydr)–hydrothermal post-treatment	Photodegradation: 96.05% (6 h) k(1st) = 0.45 min^{-1} Mineralization: 76.66% (6 h) TOC Ecotoxicity: *Staphylococcus aureus*	[130]
P-doped TiO_2	Particle size: 12 nm (TEM)Composition: anatase BET surface: 88.54 cm^2g^{-1} Band gap: 3.02 eV	Ant. Conc.: 5 ppm Cat. Conc.: 0.5 gL^{-1} Light source: visible light Cat.: PT-50 (50 mg of NaH_2PO_2)	Photodegradation: 100% (60 min) k(1st) = 0.065 min^{-1} Mineralization: 72.7% (60 min) TOC	[150]
g-C_3N_4/TiO_2/kaolinite	Composition: anatase Crystallite size: 14.21 nm TiO_2 (XRD) BET surface: 51.596 m^2g^{-1} Band gap: 2.72 eV	Medium: deionized water Ant. Conc.: 10 ppm Cat. Conc.: 2 gL^{-1} Light source: Xenon lamp with 400 nm cut-off filter, 90 $mWcm^{-2}$	Photodegradation: 92% (240 min) k(1st) = 0.00813 min^{-1} Disinfection: *Stapheylococcus aureus* Stability: 4 cycles	[151]
N-TiO_2 immobilized on glass spheres	Composition: anatase Crystallite size: 5.69 nm BET surface: 140.47 m^2g^{-1} Band gap: 2.84 eV	Ant. Conc.: 0.02 gL^{-1} Cat. Conc.: 3 gL^{-1} Light source: 500 W Xe lamp, $\lambda > 420$ nm Cat.: N/Ti weight ratio 0.34%	Photodegradation: 93.5% (90 min) k(1st) = 0.02859 min^{-1} Ecotoxicity: Toxicity Estimation Software Tool (T.E.S.T.) Stability: 5 cycles	[133]
TiO_2 P25	Particle size: 30 nm Composition: 80% anatase, 20% rutile BET surface: 50 ± 15 m^2g^{-1}	Medium: deionized water Ant. Conc.: 0.02 gL^{-1} Cat. Conc.: 0.1 gL^{-1} pH: 6.00 ± 0.10 Light source: twelve 3 W UVA/LED lamps, 365 nm, 10$mWcm^{-2}$	Photodegradation: k(1st) = 0.2217 ± 0.0179 min^{-1} Mineralization:76% (240 min) TOC	[96]
TiO_2 P25/Fe^0	-	Medium: double distilled water Ant. Conc.: 0.03 gL^{-1} Cat. Conc.: 1 gL^{-1} pH: 3.0 Light source: 10 W UV lamp, 254 nm, 2.0 Wm^{-2}	Photodegradation: 94.6% (60 min) Stability: 5 cycles	[107]

Table 4. *Cont.*

Catalyst	Characteristics	Process conditions	Performance	Ref.
$Fe_3O_4/SiO_2/TiO_2$	Particle size: 293 ± 81 nm (SEM) Composition: anatase, rutile BET surface: 19 m^2g^{-1} PZC: 3–5 Band gap: 2.8 eV	Medium: Millipore water Ant. Conc.: 0.005 gL^{-1} Cat. Conc.: 1 gL^{-1} pH: 5.5 Light source: six 8 W blacklight blue lamps, 365 nm, 1.6–1.7 $mWcm^{-2}$	Photodegradation: 95% (90 min) k(1st) = 0.032 min^{-1} Stability: 5 cycles	[152]
TiO_2 P25 immobilized on glass plates	Composition: 80% anatase, 20% rutile BET surface: 48.3 m^2g^{-1}	Medium: deionized water Ant. Conc.: 60 $\mu molL^{-1}$ Cat. Conc.: 0.75 gL^{-1} (3.8 × 48 cm rectangle glass plate with 20.5 gm^{-2} TiO_2) pH: 9 Light source: 15 W UV-C lamp, 254 nm	Photodegradation: 100% (120 min) k(1st) = 4.0×10^{-4} s^{-1}	[112]
Mono- (Au, Ag and Cu) and bi-metallic Au–Ag and Au–Cu nanoparticles deposited on TiO_2	Particle size: 2.5–4 nm Composition: anatase, brookite BET surface: 52–64 m^2g^{-1} PZC: 6.3 Band gap: 3.1–3.19 eV	Medium: tridistilled water Ant. Conc.: 0.03 gL^{-1} Cat. Conc.: 0.5 gL^{-1} Light source: 15 W UV-C low pressure Hg lamp, 254 nm, 44 Wm^{-2}; solar simulator with a 1500 W Xenon lamp, 500 Wm^{-2} Temperature: 25 °C (<35 °C under simulated sunlight) Cat.: 1.5 wt.% for Au and Ag, 1.0 wt.% for Cu (mono-metallic); 1.0 wt.% for Au and 0.5 wt.% for Ag and Cu (bi-metallic)	Photodegradation: 100% (90 min) UV-C k(1st) = 0.06 min^{-1} 1.5% Au/TiO_2 k(1st) = 0.117 min^{-1} 1.5% Ag/TiO_2 k(1st) = 0.072 min^{-1} 1.0% Cu/TiO_2 k(1st) = 0.053 min^{-1} Au-Ag/TiO_2 k(1st) = 0.099 min^{-1} Au-Cu/TiO_2 100% (240 min) simulated sunlight k(1st) = 0.042 min^{-1} 1.5% Au/TiO_2 k(1st) = 0.04 min^{-1} 1.5% Ag/TiO_2 k(1st) = 0.023 min^{-1} 1.0% Cu/TiO_2 k(1st) = 0.021 min^{-1} Au-Ag/TiO_2 k(1st) = 0.022 min^{-1} Au-Cu/TiO_2Mineralization: 100% (180 min) TOC (UV-C) 100% (360 min, bi-metallic) TOC (simulated sunlight) Ecotoxicity: *V. fischeri*, *E. coli* Stability: 3 cycles	[121]
TiO_2 P25	Particle size: 30 nm BET surface: 35–65 m^2g^{-1}	Medium: ultra-pure water Ant. Conc.: 300 μgL^{-1} Cat. Conc.: 1 gL^{-1} Light source: UV-A, 365 nm, 1.6–1.7 $mWcm^{-2}$	Photodegradation: 100% (6 min) Ecotoxicity: *Vibrio fischeri*	[132]

Table 4. *Cont.*

Catalyst	Characteristics	Process conditions	Performance	Ref.
TiO_2/MMT (montmorillonite)	Particle size: 40–60 nm Composition: anatase BET surface: 53.058 m^2g^{-1} PZC: 8.4	Ant. Conc.: 0.02 gL^{-1} Cat. Conc.: 0.1 gL^{-1} pH: 5.0 Light source: 16 W UV-C lamp	Photodegradation: 61.7% (120 min) k(1st) = 0.0069 min^{-1} $t_{1/2}$ = 100.46 min Stability: 5 cycles	[78]
TiO_2 P25	BET surface: 56 m^2g^{-1}	Ant. Conc.: 12.5 μM Cat. Conc.: 1 gL^{-1} Light source: six 8 W mercurial fluorescent tubes, UVA 365 nm, 18–19 Wm^{-2}	Photodegradation: 100% (30 min)	[153]

6. Challenges and Future Research Needs

Among the different advanced oxidation processes, heterogeneous photocatalysis over TiO_2-based materials is one of the most efficient techniques for the removal of antibiotics. However, practical application on a large scale remains a challenge. This process has great potential, but it needs to be improved and optimized to be implemented in industry. The most significant issues are outlined as follows:

- Huge variety of TiO_2-based materials with unique features have been synthesized, as well as many different techniques having been reported to synthesize efficient TiO_2-based photocatalysts. However, as the operational cost is crucial for practical applications, there is still a strong need for simple and cost-effective synthesis and modification processes to decrease the cost of the photocatalytic process. This can be achieved by implementing low-cost synthesis methods or by using low-cost materials, or both. The introduction of multiple cheaper modificators might be more cost-effective than introducing one expensive dopant, while retaining high photocatalytic activity. For example, low-cost alternatives to photocatalysts modified with expensive and scarce noble metals could be TiO_2-doped with cocatalysts like Ni and Cu [154,155] or Co and Ni [156]; Mo-doped TiO_2 [157], graphene-doped TiO_2 [158], Cu nanowires decorated with TiO_2 [159].
- Special emphasis should be placed on the development of TiO_2-based photocatalysts active under solar light. Considering that high energy costs are associated with the usage of visible and ultraviolet light sources, solar photocatalysis is not only a cost-efficient solution, but also a sustainable one. Besides, further cost reduction can be achieved through the development of highly stable photocatalysts that can be easily separated from aqueous solution (immobilized/supported catalysts) and successfully reused over multiple cycles;
- Further research is needed in studying the potential of photocatalytic process over TiO_2-based materials for the successful removal not only of antibiotics, but also of ARB and ARGs from wastewaters;
- In order to fulfill industrial application, photocatalytic tests should be carried out on real wastewater samples. The composition of wastewater is complicated: it contains a mixture of different pharmaceuticals and other organic pollutants, as well as inorganic substances. This decreases the degradation efficiency of antibiotics compared to the degradation efficiency of a single antibiotic in purified water. Moreover, there is a need to design and develop pilot plant installations that work under solar irradiation and in the continuous mode of operation. These are essential requirements for industrial treatment systems;
- Further investigations should be performed on the efficiency of combined methods. Heterogeneous photocatalysis combined with conventional treatment methods, for example with biological treatment, should be studied in order to develop a technically feasible and cost-effective solution for wastewater treatment;

- Assessment of eco-toxicity should be an essential part of degradation tests over TiO_2-based photocatalysts. The complete mineralization of antibiotics remains a challenge, and incomplete mineralization leads to the formation of various intermediates and by-products, sometimes more toxic than the parent compound. Degradation mechanisms require deeper studies.

7. Conclusions

The current review focuses on the recent progress in the photocatalytic removal of antibiotics over TiO_2 and TiO_2-based materials. Heterogeneous photocatalysis has shown huge potential as an efficient, cost-effective and energy-efficient advanced oxidation process that is able to utilize the green and sustainable source of light – solar irradiation. The global occurrence of antibiotics in the environment, their fate and harmful effects on ecosystems and human health have been covered by the present review. Special emphasis is given to sulfamethoxazole, trimethoprim and ciprofloxacin as the most commonly detected antibiotics in different aquatic systems, raising significant concerns. The huge need for antibiotics removal from contaminated waters has been highlighted. Since conventional wastewater treatment fails to remove such complicated pharmaceuticals pollutants, various antibiotic removal technologies have been briefly discussed. The fundamentals of photocatalytic process over TiO_2 have been presented, along with the modification methods of TiO_2 to overcome its limitations and enhance efficiency. The photocatalytic performance of various TiO_2 and TiO_2-based materials and the effect of different process parameters (amounts of pollutant and photocatalyst, pH, light, reaction media, presence of inorganic ions, natural organic matter and oxidants) have been the main focus of this review. Summarizing recent progress in the photocatalytic removal of the three widespread antibiotics, heterogeneous photocatalysis over TiO_2-based materials has demonstrated its high potential for industry applications. We believe that the present review will contribute to the further progress in the design and development of efficient and cost-effective TiO_2-based photocatalytic systems to meet the outlined challenges of large-scale application.

Author Contributions: Conceptualization, A.K. and T.D.; investigation, A.K.; resources, W.K.; data curation, A.K.; writing—original draft preparation, A.K.; writing—review and editing, T.D. and W.K.; visualization, A.K.; supervision, T.D. and W.K. All authors have read and agreed to the published version of the manuscript.

Funding: This research received no external funding.

Data Availability Statement: The data presented in this study are available in Application of TiO_2-based Photocatalysts to Antibiotics Degradation: Cases of Sulfamethoxazole, Trimethoprim and Ciprofloxacin.

Acknowledgments: Anastasiya Kutuzova would like to gratefully acknowledge scientific support by Matthias Beller and Jennifer Strunk, LIKAT, and the grant from Erasmus+ Program-International Credit Mobility project # 2019-1-IE02-KA107-000650 funded by the European Commission that made it possible to work at the University of Limerick, Ireland.

Conflicts of Interest: The authors declare no conflict of interest.

Abbreviations

AMR	antimicrobial resistance
AOPs	advanced oxidation processes
APIs	active pharmaceutical ingredients
ARB	antibiotic resistant bacteria
ARGs	antibiotic resistant genes
BET	Brunauer-Emmett-Teller
CB	conduction band
CIP	ciprofloxacin
COD	chemical oxygen demand
DOC	dissolved organic carbon
NOM	natural organic matter
NPOC	non-purgeable organic carbon
PZC	point of zero charge
SEM	scanning electron microscopy
SMX	sulfamethoxazole
TEM	transmission electron microscopy
TMP	trimethoprim
TOC	total organic carbon
UV	ultraviolet
VB	valence band
WWTP	wastewater treatment plant
XRD	X-ray diffraction

References

1. OECD. *Pharmaceutical Residues in Freshwater: Hazards and Policy Responses*; OECD Publishing: Paris, France, 2019; ISBN 9789264776333.
2. Chavoshani, A.; Hashemi, M.; Mehdi Amin, M.; Ameta, S.C. Pharmaceuticals as emerging micropollutants in aquatic environments. In *Micropollutants and Challenges*; Elsevier Inc.: Philadelphia, PA, USA, 2020; pp. 35–90. ISBN 9780128186121.
3. Aus der Beek, T.; Weber, F.A.; Bergmann, A.; Hickmann, S.; Ebert, I.; Hein, A.; Küster, A. Pharmaceuticals in the environment-Global occurrences and perspectives. *Environ. Toxicol. Chem.* **2016**, *35*, 823–835. [CrossRef]
4. Carvalho, I.T.; Santos, L. Antibiotics in the aquatic environments: A review of the European scenario. *Environ. Int.* **2016**, *94*, 736–757. [CrossRef] [PubMed]
5. Bungau, S.; Tit, D.M.; Behl, T.; Aleya, L.; Zaha, D.C. Aspects of excessive antibiotic consumption and environmental influences correlated with the occurrence of resistance to antimicrobial agents. *Curr. Opin. Environ. Sci. Health* **2021**, *19*, 100224. [CrossRef]
6. Zainab, S.M.; Junaid, M.; Xu, N.; Malik, R.N. Antibiotics and antibiotic resistant genes (ARGs) in groundwater: A global review on dissemination, sources, interactions, environmental and human health risks. *Water Res.* **2020**, *187*, 116455. [CrossRef] [PubMed]
7. Kümmerer, K. The presence of pharmaceuticals in the environment due to human use—Present knowledge and future challenges. *J. Environ. Manag.* **2009**, *90*, 2354–2366. [CrossRef]
8. Szymańska, U.; Wiergowski, M.; Sołtyszewski, I.; Kuzemko, J.; Wiergowska, G.; Woźniak, M.K. Presence of antibiotics in the aquatic environment in Europe and their analytical monitoring: Recent trends and perspectives. *Microchem. J.* **2019**, *147*, 729–740. [CrossRef]
9. Bilal, M.; Mehmood, S.; Rasheed, T.; Iqbal, H.M.N. Antibiotics traces in the aquatic environment: Persistence and adverse environmental impact. *Curr. Opin. Environ. Sci. Health* **2020**, *13*, 68–74. [CrossRef]
10. Felis, E.; Kalka, J.; Sochacki, A.; Kowalska, K.; Bajkacz, S.; Harnisz, M.; Korzeniewska, E. Antimicrobial pharmaceuticals in the aquatic environment-occurrence and environmental implications. *Eur. J. Pharmacol.* **2020**, *866*, 172813. [CrossRef]
11. Kümmerer, K. Antibiotics in the aquatic environment—A review—Part I. *Chemosphere* **2009**, *75*, 417–434. [CrossRef]
12. Danner, M.C.; Robertson, A.; Behrends, V.; Reiss, J. Antibiotic pollution in surface fresh waters: Occurrence and effects. *Sci. Total Environ.* **2019**, *664*, 793–804. [CrossRef]
13. Menz, J.; Olsson, O.; Kümmerer, K. Antibiotic residues in livestock manure: Does the EU risk assessment sufficiently protect against microbial toxicity and selection of resistant bacteria in the environment? *J. Hazard. Mater.* **2019**, *379*, 120807. [CrossRef]
14. Singh, R.; Singh, A.P.; Kumar, S.; Giri, B.S.; Kim, K.H. Antibiotic resistance in major rivers in the world: A systematic review on occurrence, emergence, and management strategies. *J. Clean. Prod.* **2019**, *234*, 1484–1505. [CrossRef]
15. Rodriguez-Mozaz, S.; Vaz-Moreira, I.; Varela Della Giustina, S.; Llorca, M.; Barceló, D.; Schubert, S.; Berendonk, T.U.; Michael-Kordatou, I.; Fatta-Kassinos, D.; Martinez, J.L.; et al. Antibiotic residues in final effluents of European wastewater treatment plants and their impact on the aquatic environment. *Environ. Int.* **2020**, *140*, 105733. [CrossRef]
16. Kovalakova, P.; Cizmas, L.; McDonald, T.J.; Marsalek, B.; Feng, M.; Sharma, V.K. Occurrence and toxicity of antibiotics in the aquatic environment: A review. *Chemosphere* **2020**, *251*, 126351. [CrossRef]

17. Sabri, N.A.; van Holst, S.; Schmitt, H.; van der Zaan, B.M.; Gerritsen, H.W.; Rijnaarts, H.H.M.; Langenhoff, A.A.M. Fate of antibiotics and antibiotic resistance genes during conventional and additional treatment technologies in wastewater treatment plants. *Sci. Total Environ.* **2020**, *741*, 140199. [CrossRef]
18. Prashanth, V.; Jayasree, P.; Rajput, P.; Remya, N. Solar photocatalysis and its application for emerging contaminant removal from wastewater. In *Advanced Oxidation Processes for Effluent Treatment Plants*; Elsevier Inc.: Philadelphia, PA, USA, 2021; pp. 69–85. ISBN 9780128210116.
19. Majumder, A.; Gupta, B.; Gupta, A.K. Pharmaceutically active compounds in aqueous environment: A status, toxicity and insights of remediation. *Environ. Res.* **2019**, *176*, 108542. [CrossRef]
20. Johnson, A.C.; Keller, V.; Dumont, E.; Sumpter, J.P. Assessing the concentrations and risks of toxicity from the antibiotics ciprofloxacin, sulfamethoxazole, trimethoprim and erythromycin in European rivers. *Sci. Total Environ.* **2015**, *511*, 747–755. [CrossRef]
21. Kötke, D.; Gandrass, J.; Xie, Z.; Ebinghaus, R. Prioritised pharmaceuticals in German estuaries and coastal waters: Occurrence and environmental risk assessment. *Environ. Pollut.* **2019**, *255*, 113161. [CrossRef]
22. Fekadu, S.; Alemayehu, E.; Dewil, R.; Van der Bruggen, B. Pharmaceuticals in freshwater aquatic environments: A comparison of the African and European challenge. *Sci. Total Environ.* **2019**, *654*, 324–337. [CrossRef]
23. Prasannamedha, G.; Kumar, P.S. A review on contamination and removal of sulfamethoxazole from aqueous solution using cleaner techniques: Present and future perspective. *J. Clean. Prod.* **2020**, *250*, 119553. [CrossRef]
24. Sarafraz, M.; Sadeghi, M.; Yazdanbakhsh, A.; Amini, M.M.; Sadani, M.; Eslami, A. Enhanced photocatalytic degradation of ciprofloxacin by black Ti3+/N-TiO_2 under visible LED light irradiation: Kinetic, energy consumption, degradation pathway, and toxicity assessment. *Process Saf. Environ. Prot.* **2020**, *137*, 261–272. [CrossRef]
25. Ryan, C.C.; Tan, D.T.; Arnold, W.A. Direct and indirect photolysis of sulfamethoxazole and trimethoprim in wastewater treatment plant effluent. *Water Res.* **2011**, *45*, 1280–1286. [CrossRef]
26. Oros-Ruiz, S.; Zanella, R.; Prado, B. Photocatalytic degradation of trimethoprim by metallic nanoparticles supported on TiO_2-P25. *J. Hazard. Mater.* **2013**, *263*, 28–35. [CrossRef]
27. Paul, T.; Dodd, M.C.; Strathmann, T.J. Photolytic and photocatalytic decomposition of aqueous ciprofloxacin: Transformation products and residual antibacterial activity. *Water Res.* **2010**, *44*, 3121–3132. [CrossRef]
28. Jia, A.; Wan, Y.; Xiao, Y.; Hu, J. Occurrence and fate of quinolone and fluoroquinolone antibiotics in a municipal sewage treatment plant. *Water Res.* **2012**, *46*, 387–394. [CrossRef]
29. Haddad, T.; Kümmerer, K. Characterization of photo-transformation products of the antibiotic drug Ciprofloxacin with liquid chromatography-tandem mass spectrometry in combination with accurate mass determination using an LTQ-Orbitrap. *Chemosphere* **2014**, *115*, 40–46. [CrossRef]
30. Kumar, M.; Jaiswal, S.; Sodhi, K.K.; Shree, P.; Singh, D.K.; Agrawal, P.K.; Shukla, P. Antibiotics bioremediation: Perspectives on its ecotoxicity and resistance. *Environ. Int.* **2019**, *124*, 448–461. [CrossRef]
31. Girardi, C.; Greve, J.; Lamshöft, M.; Fetzer, I.; Miltner, A.; Schäffer, A.; Kästner, M. Biodegradation of ciprofloxacin in water and soil and its effects on the microbial communities. *J. Hazard. Mater.* **2011**, *198*, 22–30. [CrossRef]
32. Cortes, L.G.; Marinov, D.; Sanseverino, I.; Cuenca, A.N.; Niegowska, M.; Rodriguez, E.P.; Lettieri, T. *Selection of Substances for the 3rd Watch List under the Water Framework Directive*; Office of the European Union: Luxembourg, 2020.
33. Mezzelani, M.; Gorbi, S.; Regoli, F. Pharmaceuticals in the aquatic environments: Evidence of emerged threat and future challenges for marine organisms. *Mar. Environ. Res.* **2018**, *140*, 41–60. [CrossRef] [PubMed]
34. Savin, M.; Bierbaum, G.; Hammerl, J.A.; Heinemann, C.; Parcina, M.; Sib, E.; Voigt, A.; Kreyenschmidt, J. Antibiotic-resistant bacteria and antimicrobial residues in wastewater and process water from German pig slaughterhouses and their receiving municipal wastewater treatment plants. *Sci. Total Environ.* **2020**, *727*, 138788. [CrossRef]
35. Bartolomeu, M.; Neves, M.G.P.M.S.; Faustino, M.A.F.; Almeida, A. Wastewater chemical contaminants: Remediation by advanced oxidation processes. *Photochem. Photobiol. Sci.* **2018**, *17*, 1573–1598. [CrossRef] [PubMed]
36. Li, L.G.; Huang, Q.; Yin, X.; Zhang, T. Source tracking of antibiotic resistance genes in the environment—Challenges, progress, and prospects. *Water Res.* **2020**, *185*, 116127. [CrossRef] [PubMed]
37. Prieto-Rodriguez, L.; Miralles-Cuevas, S.; Oller, I.; Agüera, A.; Puma, G.L.; Malato, S. Treatment of emerging contaminants in wastewater treatment plants (WWTP) effluents by solar photocatalysis using low TiO_2 concentrations. *J. Hazard. Mater.* **2012**, *211–212*, 131–137. [CrossRef]
38. Baran, W.; Adamek, E.; Ziemiańska, J.; Sobczak, A. Effects of the presence of sulfonamides in the environment and their influence on human health. *J. Hazard. Mater.* **2011**, *196*, 1–15. [CrossRef]
39. Cheng, D.; Ngo, H.H.; Guo, W.; Chang, S.W.; Nguyen, D.D.; Liu, Y.; Wei, Q.; Wei, D. A critical review on antibiotics and hormones in swine wastewater: Water pollution problems and control approaches. *J. Hazard. Mater.* **2020**, *387*, 121682. [CrossRef]
40. Miranda-García, N.; Suárez, S.; Sánchez, B.; Coronado, J.M.; Malato, S.; Maldonado, M.I. Photocatalytic degradation of emerging contaminants in municipal wastewater treatment plant effluents using immobilized TiO_2 in a solar pilot plant. *Appl. Catal. B Environ.* **2011**, *103*, 294–301. [CrossRef]
41. Chaturvedi, P.; Giri, B.S.; Shukla, P.; Gupta, P. Recent advancement in remediation of synthetic organic antibiotics from environmental matrices: Challenges and perspective. *Bioresour. Technol.* **2021**, *319*, 124161. [CrossRef]

42. Phoon, B.L.; Ong, C.C.; Mohamed Saheed, M.S.; Show, P.L.; Chang, J.S.; Ling, T.C.; Lam, S.S.; Juan, J.C. Conventional and emerging technologies for removal of antibiotics from wastewater. *J. Hazard. Mater.* **2020**, *400*, 122961. [CrossRef]
43. Taoufik, N.; Boumya, W.; Janani, F.Z.; Elhalil, A.; Mahjoubi, F.Z.; Barka, N. Removal of emerging pharmaceutical pollutants: A systematic mapping study review. *J. Environ. Chem. Eng.* **2020**, *8*, 104251. [CrossRef]
44. Varma, K.S.; Tayade, R.J.; Shah, K.J.; Joshi, P.A.; Shukla, A.D.; Gandhi, V.G. Photocatalytic degradation of pharmaceutical and pesticide compounds (PPCs) using doped TiO_2 nanomaterials: A review. *Water-Energy Nexus* **2020**, *3*, 46–61. [CrossRef]
45. Majumdar, A.; Pal, A. Recent advancements in visible-light-assisted photocatalytic removal of aqueous pharmaceutical pollutants. *Clean Technol. Environ. Policy* **2020**, *22*, 11–42. [CrossRef]
46. Lu, Z.Y.; Ma, Y.L.; Zhang, J.T.; Fan, N.S.; Huang, B.C.; Jin, R.C. A critical review of antibiotic removal strategies: Performance and mechanisms. *J. Water Process Eng.* **2020**, *38*, 101681. [CrossRef]
47. Fawzi Suleiman Khasawneh, O.; Palaniandy, P. Photocatalytic Degradation of Pharmaceuticals Using TiO_2 Based Nanocomposite Catalyst-Review. *Civ. Environ. Eng. Reports* **2019**, *29*, 1–33. [CrossRef]
48. Hiller, C.X.; Hübner, U.; Fajnorova, S.; Schwartz, T.; Drewes, J.E. Antibiotic microbial resistance (AMR) removal efficiencies by conventional and advanced wastewater treatment processes: A review. *Sci. Total Environ.* **2019**, *685*, 596–608. [CrossRef]
49. Anjali, R.; Shanthakumar, S. Insights on the current status of occurrence and removal of antibiotics in wastewater by advanced oxidation processes. *J. Environ. Manag.* **2019**, *246*, 51–62. [CrossRef]
50. Serhiienko, A.O.; Dontsova, T.A.; Yanushevska, O.I.; Nahirniak, S.V.; Hosseini-Bandegharaei, A. Ceramic Membranes: New Trends and Prospects. *Water Water Purif. Technol. Sci. Tech. News* **2020**, *27*, 4–31. [CrossRef]
51. Chen, D.; Cheng, Y.; Zhou, N.; Chen, P.; Wang, Y.; Li, K.; Huo, S.; Cheng, P.; Peng, P.; Zhang, R.; et al. Photocatalytic degradation of organic pollutants using TiO_2-based photocatalysts: A review. *J. Clean. Prod.* **2020**, *268*, 121725. [CrossRef]
52. Lee, C.M.; Palaniandy, P.; Dahlan, I. Pharmaceutical residues in aquatic environment and water remediation by TiO_2 heterogeneous photocatalysis: A review. *Environ. Earth Sci.* **2017**, *76*, 611. [CrossRef]
53. Wang, J.; Zhuan, R. Degradation of antibiotics by advanced oxidation processes: An overview. *Sci. Total Environ.* **2020**, *701*, 135023. [CrossRef]
54. Byrne, C.; Subramanian, G.; Pillai, S.C. Recent advances in photocatalysis for environmental applications. *J. Environ. Chem. Eng.* **2018**, *6*, 3531–3555. [CrossRef]
55. Ribeiro, A.R.; Nunes, O.C.; Pereira, M.F.R.; Silva, A.M.T. An overview on the advanced oxidation processes applied for the treatment of water pollutants defined in the recently launched Directive 2013/39/EU. *Environ. Int.* **2015**, *75*, 33–51. [CrossRef]
56. Wei, Z.; Liu, J.; Shangguan, W. A review on photocatalysis in antibiotic wastewater: Pollutant degradation and hydrogen production. *Chin. J. Catal.* **2020**, *41*, 1440–1450. [CrossRef]
57. Giwa, A.; Yusuf, A.; Balogun, H.A.; Sambudi, N.S.; Bilad, M.R.; Adeyemi, I.; Chakraborty, S.; Curcio, S. Recent advances in advanced oxidation processes for removal of contaminants from water: A comprehensive review. *Process Saf. Environ. Prot.* **2021**, *146*, 220–256. [CrossRef]
58. Kutuzova, A.; Dontsova, T. Synthesis, characterization and properties of titanium dioxide obtained by hydrolytic method. In Proceedings of the IEEE 7th International Conference on Nanomaterials: Applications and Properties, NAP 2017 IEEE, Odessa, Ukraine, 10–15 September 2017; pp. 01NNPT02-1–01NNPT02-5.
59. Sviderskyi, A.; Nahirniak, S.; Yashchenko, T.; Dontsova, T.; Kalinowski, S. Properties of TiO_2 and SnO_2 in a State of Different Dispersion and Morphology. In Proceedings of the IEEE 8th International Conference Nanomaterials: Application & Properties (NAP), Zatoka, Ukraine, 9–14 September 2018; pp. 1–4.
60. Dontsova, T.A.; Kutuzova, A.S.; Bila, K.O.; Kyrii, S.O.; Kosogina, I.V.; Nechyporuk, D.O. Enhanced Photocatalytic Activity of TiO_2/SnO_2 Binary Nanocomposites. *J. Nanomater.* **2020**, *2020*, 1–13. [CrossRef]
61. Kutuzova, A.S.; Dontsova, T.A. Characterization and properties of TiO_2–SnO_2 nanocomposites, obtained by hydrolysis method. *Appl. Nanosci.* **2019**, *9*, 873–880. [CrossRef]
62. Gopinath, K.P.; Madhav, N.V.; Krishnan, A.; Malolan, R.; Rangarajan, G. Present applications of titanium dioxide for the photocatalytic removal of pollutants from water: A review. *J. Environ. Manag.* **2020**, *270*, 110906. [CrossRef]
63. Wen, J.; Li, X.; Liu, W.; Fang, Y.; Xie, J.; Xu, Y. Photocatalysis fundamentals and surface modification of TiO_2 nanomaterials. *Cuihua Xuebao Chin. J. Catal.* **2015**, *36*, 2049–2070. [CrossRef]
64. Kumar, A.; Khan, M.; He, J.; Lo, I.M.C. Recent developments and challenges in practical application of visible–light–driven TiO_2–based heterojunctions for PPCP degradation: A critical review. *Water Res.* **2020**, *170*, 115356. [CrossRef]
65. Kutuzova, A.; Dontsova, T.; Kwapinski, W. TiO_2–SnO_2 Nanocomposites: Effect of Acid–Base and Structural-Adsorption Properties on Photocatalytic Performance. *J. Inorg. Organomet. Polym. Mater.* **2020**, *30*, 3060–3072. [CrossRef]
66. Abdurahman, M.H.; Abdullah, A.Z.; Shoparwe, N.F. A comprehensive review on sonocatalytic, photocatalytic, and sonophotocatalytic processes for the degradation of antibiotics in water: Synergistic mechanism and degradation pathway. *Chem. Eng. J.* **2020**, 127412. [CrossRef]
67. Kutuzova, A.; Dontsova, T. TiO_2-SnO_2 Nanocomposites Obtained by Hydrothermal Method. In Proceedings of the IEEE 8th International Conference on Nanomaterials: Applications & Properties, Zatoka, Ukraine, 9–14 September 2018; pp. 1–5.
68. Bila, K.; Dontsova, T.; Kutuzova, A. Effect of Precursor Type on Physico-chemical and Photocatalytic Properties of TiO_2-SnO_2 Nanocomposites. In Proceedings of the IEEE 10th International Conference on "Nanomaterials: Applications and Properties", NAP 2020 IEEE, Sumy, Ukraine, 9–13 November 2020; pp. 02NEE01-1–02NEE01-4.

69. Fagan, R.; McCormack, D.E.; Dionysiou, D.D.; Pillai, S.C. A review of solar and visible light active TiO_2 photocatalysis for treating bacteria, cyanotoxins and contaminants of emerging concern. *Mater. Sci. Semicond. Process.* **2016**, *42*, 2–14. [CrossRef]
70. Dong, H.; Zeng, G.; Tang, L.; Fan, C.; Zhang, C.; He, X.; He, Y. An overview on limitations of TiO_2-based particles for photocatalytic degradation of organic pollutants and the corresponding countermeasures. *Water Res.* **2015**, *79*, 128–146. [CrossRef]
71. Wetchakun, K.; Wetchakun, N.; Sakulsermsuk, S. An overview of solar/visible light-driven heterogeneous photocatalysis for water purification: TiO_2- and ZnO-based photocatalysts used in suspension photoreactors. *J. Ind. Eng. Chem.* **2019**, *71*, 19–49. [CrossRef]
72. Tiwari, A.; Shukla, A.; Lalliansanga; Tiwari, D.; Lee, S.M. Nanocomposite thin films Ag0(NP)/TiO_2 in the efficient removal of micro-pollutants from aqueous solutions: A case study of tetracycline and sulfamethoxazole removal. *J. Environ. Manag.* **2018**, *220*, 96–108. [CrossRef]
73. Alfred, M.O.; Omorogie, M.O.; Bodede, O.; Moodley, R.; Ogunlaja, A.; Adeyemi, O.G.; Günter, C.; Taubert, A.; Iermak, I.; Eckert, H.; et al. Solar-active clay-TiO_2 nanocomposites prepared via biomass assisted synthesis: Efficient removal of ampicillin, sulfamethoxazole and artemether from water. *Chem. Eng. J.* **2020**, *398*, 125544. [CrossRef]
74. Ioannidou, E.; Frontistis, Z.; Antonopoulou, M.; Venieri, D.; Konstantinou, I.; Kondarides, D.I.; Mantzavinos, D. Solar photocatalytic degradation of sulfamethoxazole over tungsten—Modified TiO_2. *Chem. Eng. J.* **2017**, *318*, 143–152. [CrossRef]
75. Cai, Q.; Hu, J. Decomposition of sulfamethoxazole and trimethoprim by continuous UVA/LED/TiO_2 photocatalysis: Decomposition pathways, residual antibacterial activity and toxicity. *J. Hazard. Mater.* **2017**, *323*, 527–536. [CrossRef]
76. Karim, A.V.; Shriwastav, A. Degradation of ciprofloxacin using photo, sono, and sonophotocatalytic oxidation with visible light and low-frequency ultrasound: Degradation kinetics and pathways. *Chem. Eng. J.* **2020**, *392*, 124853. [CrossRef]
77. Wu, Z.; Liang, Y.; Yuan, X.; Zou, D.; Fang, J.; Jiang, L.; Zhang, J.; Yang, H.; Xiao, Z. MXene Ti_3C_2 derived Z–scheme photocatalyst of graphene layers anchored TiO_2/g–C_3N_4 for visible light photocatalytic degradation of refractory organic pollutants. *Chem. Eng. J.* **2020**, *394*, 124921. [CrossRef]
78. Hassani, A.; Khataee, A.; Karaca, S. Photocatalytic degradation of ciprofloxacin by synthesized TiO_2 nanoparticles on montmorillonite: Effect of operation parameters and artificial neural network modeling. *J. Mol. Catal. A Chem.* **2015**, *409*, 149–161. [CrossRef]
79. Xie, X.; Li, S.; Zhang, H.; Wang, Z.; Huang, H. Promoting charge separation of biochar-based Zn-TiO_2/pBC in the presence of ZnO for efficient sulfamethoxazole photodegradation under visible light irradiation. *Sci. Total Environ.* **2019**, *659*, 529–539. [CrossRef]
80. Zhang, H.; Wang, Z.; Li, R.; Guo, J.; Li, Y.; Zhu, J.; Xie, X. TiO_2 supported on reed straw biochar as an adsorptive and photocatalytic composite for the efficient degradation of sulfamethoxazole in aqueous matrices. *Chemosphere* **2017**, *185*, 351–360. [CrossRef]
81. Kim, J.R.; Kan, E. Heterogeneous photocatalytic degradation of sulfamethoxazole in water using a biochar-supported TiO_2 photocatalyst. *J. Environ. Manag.* **2016**, *180*, 94–101. [CrossRef]
82. Chiang, L.F.; Doong, R.A. Enhanced photocatalytic degradation of sulfamethoxazole by visible-light-sensitive TiO_2 with low Cu addition. *Sep. Purif. Technol.* **2015**, *156*, 1003–1010. [CrossRef]
83. Abellán, M.N.; Giménez, J.; Esplugas, S. Photocatalytic degradation of antibiotics: The case of sulfamethoxazole and trimethoprim. *Catal. Today* **2009**, *144*, 131–136. [CrossRef]
84. Yuan, R.; Zhu, Y.; Zhou, B.; Hu, J. Photocatalytic oxidation of sulfamethoxazole in the presence of TiO_2: Effect of matrix in aqueous solution on decomposition mechanisms. *Chem. Eng. J.* **2019**, *359*, 1527–1536. [CrossRef]
85. Nasuhoglu, D.; Yargeau, V.; Berk, D. Photo-removal of sulfamethoxazole (SMX) by photolytic and photocatalytic processes in a batch reactor under UV-C radiation (λmax = 254 nm). *J. Hazard. Mater.* **2011**, *186*, 67–75. [CrossRef]
86. Gong, H.; Chu, W. Determination and toxicity evaluation of the generated products in sulfamethoxazole degradation by UV/$CoFe_2O_4$/TiO_2. *J. Hazard. Mater.* **2016**, *314*, 197–203. [CrossRef]
87. Choi, J.; Lee, H.; Choi, Y.; Kim, S.; Lee, S.; Lee, S.; Choi, W.; Lee, J. Heterogeneous photocatalytic treatment of pharmaceutical micropollutants: Effects of wastewater effluent matrix and catalyst modifications. *Appl. Catal. B Environ.* **2014**, *147*, 8–16. [CrossRef]
88. Sarkar, S.; Das, R.; Choi, H.; Bhattacharjee, C. Involvement of process parameters and various modes of application of TiO_2 nanoparticles in heterogeneous photocatalysis of pharmaceutical wastes—A short review. *RSC Adv.* **2014**, *4*, 57250–57266. [CrossRef]
89. Wang, N.; Li, X.; Yang, Y.; Zhou, Z.; Shang, Y.; Zhuang, X. Photocatalytic degradation of sulfonamides by Bi2O3-TiO_2/PAC ternary composite: Mechanism, degradation pathway. *J. Water Process Eng.* **2020**, *36*, 101335. [CrossRef]
90. Mourid, E.H.; El Mouchtari, E.M.; El Mersly, L.; Benaziz, L.; Rafqah, S.; Lakraimi, M. Development of a new recyclable nanocomoposite LDH-TiO_2 for the degradation of antibiotic sulfamethoxazole under UVA radiation: An approach towards sunlight. *J. Photochem. Photobiol. A Chem.* **2020**, *396*, 112530. [CrossRef]
91. Długosz, M.; Zmudzki, P.; Kwiecień, A.; Szczubiałka, K.; Krzek, J.; Nowakowska, M. Photocatalytic degradation of sulfamethoxazole in aqueous solution using a floating TiO_2-expanded perlite photocatalyst. *J. Hazard. Mater.* **2015**, *298*, 146–153. [CrossRef]
92. De Matos Rodrigues, M.H.; Rodrigues de Sousa, P.A.; Borges, K.C.M.; de Melo Coelho, L.; de Fátima Gonçalves, R.; Teodoro, M.D.; Vilella da Motta, F.; Maribondo do Nascimento, R.; Júnior, M.G. Enhanced degradation of the antibiotic sulfamethoxazole by heterogeneous photocatalysis using $Ce_{0,8}Gd_{0,2}O_{2-\delta}$/$TiO_2$ particles. *J. Alloys Compd.* **2019**, *808*, 2–10. [CrossRef]

93. Luo, X.; Zheng, Z.; Greaves, J.; Cooper, W.J.; Song, W. Trimethoprim: Kinetic and mechanistic considerations in photochemical environmental fate and AOP treatment. *Water Res.* **2012**, *46*, 1327–1336. [CrossRef]
94. Hu, K.; Li, R.; Ye, C.; Wang, A.; Wei, W.; Hu, D.; Qiu, R.; Yan, K. Facile synthesis of Z-scheme composite of TiO_2 nanorod/g-C3N4 nanosheet efficient for photocatalytic degradation of ciprofloxacin. *J. Clean. Prod.* **2020**, *253*, 120055. [CrossRef]
95. Gad-Allah, T.A.; Ali, M.E.M.; Badawy, M.I. Photocatalytic oxidation of ciprofloxacin under simulated sunlight. *J. Hazard. Mater.* **2011**, *186*, 751–755. [CrossRef]
96. Li, S.; Hu, J. Transformation products formation of ciprofloxacin in UVA/LED and UVA/LED/TiO_2 systems: Impact of natural organic matter characteristics. *Water Res.* **2018**, *132*, 320–330. [CrossRef]
97. Li, Y.; Fu, Y.; Zhu, M. Green synthesis of 3D tripyramid TiO_2 architectures with assistance of aloe extracts for highly efficient photocatalytic degradation of antibiotic ciprofloxacin. *Appl. Catal. B Environ.* **2020**, *260*, 118149. [CrossRef]
98. Huang, X.; Yang, W.; Zhang, G.; Yan, L.; Zhang, Y.; Jiang, A.; Xu, H.; Zhou, M.; Liu, Z.; Tang, H.; et al. Alternative synthesis of nitrogen and carbon co-doped TiO_2 for removing fluoroquinolone antibiotics in water under visible light. *Catal. Today* **2021**, *361*, 11–16. [CrossRef]
99. Du, J.; Ma, S.; Yan, Y.; Li, K.; Zhao, F.; Zhou, J. Corn-silk-templated synthesis of TiO_2 nanotube arrays with Ag_3PO_4 nanoparticles for efficient oxidation of organic pollutants and pathogenic bacteria under solar light. *Colloids Surf. A Physicochem. Eng. Asp.* **2019**, *572*, 237–249. [CrossRef]
100. Gan, Y.; Zhang, M.; Xiong, J.; Zhu, J.; Li, W.; Zhang, C.; Cheng, G. Impact of Cu particles on adsorption and photocatalytic capability of mesoporous Cu@TiO_2 hybrid towards ciprofloxacin antibiotic removal. *J. Taiwan Inst. Chem. Eng.* **2019**, *96*, 229–242. [CrossRef]
101. Awfa, D.; Ateia, M.; Fujii, M.; Yoshimura, C. Novel Magnetic Carbon Nanotube-TiO_2 Composites for Solar Light Photocatalytic Degradation of Pharmaceuticals in the Presence of Natural Organic Matter. *J. Water Process Eng.* **2019**, *31*, 100836. [CrossRef]
102. Carbajo, J.; Jiménez, M.; Miralles, S.; Malato, S.; Faraldos, M.; Bahamonde, A. Study of application of titania catalysts on solar photocatalysis: Influence of type of pollutants and water matrices. *Chem. Eng. J.* **2016**, *291*, 64–73. [CrossRef]
103. Malesic-Eleftheriadou, N.; Evgenidou, E.; Kyzas, G.Z.; Bikiaris, D.N.; Lambropoulou, D.A. Removal of antibiotics in aqueous media by using new synthesized bio-based poly (ethylene terephthalate)-TiO_2 photocatalysts. *Chemosphere* **2019**, *234*, 746–755. [CrossRef]
104. Porcar-Santos, O.; Cruz-Alcalde, A.; López-Vinent, N.; Zanganas, D.; Sans, C. Photocatalytic degradation of sulfamethoxazole using TiO_2 in simulated seawater: Evidence for direct formation of reactive halogen species and halogenated by-products. *Sci. Total Environ.* **2020**, *736*, 139605. [CrossRef]
105. Yang, C.C.; Huang, C.L.; Cheng, T.C.; Lai, H.T. Inhibitory effect of salinity on the photocatalytic degradation of three sulfonamide antibiotics. *Int. Biodeterior. Biodegrad.* **2015**, *102*, 116–125. [CrossRef]
106. Xekoukoulotakis, N.P.; Drosou, C.; Brebou, C.; Chatzisymeon, E.; Hapeshi, E.; Fatta-Kassinos, D.; Mantzavinos, D. Kinetics of UV-A/TiO_2 photocatalytic degradation and mineralization of the antibiotic sulfamethoxazole in aqueous matrices. *Catal. Today* **2011**, *161*, 163–168. [CrossRef]
107. Diao, Z.H.; Xu, X.R.; Jiang, D.; Liu, J.J.; Kong, L.J.; Li, G.; Zuo, L.Z.; Wu, Q.H. Simultaneous photocatalytic Cr(VI) reduction and ciprofloxacin oxidation over TiO_2/Fe0 composite under aerobic conditions: Performance, durability, pathway and mechanism. *Chem. Eng. J.* **2017**, *315*, 167–176. [CrossRef]
108. Khan, S.A.; Arshad, Z.; Shahid, S.; Arshad, I.; Rizwan, K.; Sher, M.; Fatima, U. Synthesis of TiO_2/Graphene oxide nanocomposites for their enhanced photocatalytic activity against methylene blue dye and ciprofloxacin. *Compos. Part B Eng.* **2019**, *175*, 107120. [CrossRef]
109. Huerta-Aguilar, C.A.; García Gutiérrez, Y.S.; Thangarasu, P. Crystal plane directed interaction of TiO_2 [1 0 1] with AgNPs [1 1 1] silver nanoparticles enhancing solar light induced photo-catalytic oxidation of ciprofloxacin: Experimental and theoretical studies. *Chem. Eng. J.* **2020**, *394*, 124286. [CrossRef]
110. Pablos, C.; Marugán, J.; van Grieken, R.; Serrano, E. Emerging micropollutant oxidation during disinfection processes using UV-C, UV-C/H2O2, UV-A/TiO_2 and UV-A/TiO_2/$H2O_2$. *Water Res.* **2013**, *47*, 1237–1245. [CrossRef]
111. Biancullo, F.; Moreira, N.F.F.; Ribeiro, A.R.; Manaia, C.M.; Faria, J.L.; Nunes, O.C.; Castro-Silva, S.M.; Silva, A.M.T. Heterogeneous photocatalysis using UVA-LEDs for the removal of antibiotics and antibiotic resistant bacteria from urban wastewater treatment plant effluents. *Chem. Eng. J.* **2019**, *367*, 304–313. [CrossRef]
112. Salma, A.; Thoröe-Boveleth, S.; Schmidt, T.C.; Tuerk, J. Dependence of transformation product formation on pH during photolytic and photocatalytic degradation of ciprofloxacin. *J. Hazard. Mater.* **2016**, *313*, 49–59. [CrossRef] [PubMed]
113. Khan, H.; Berk, D. Characterization and mechanistic study of Mo+6 and V+5 codoped TiO_2 as a photocatalyst. *J. Photochem. Photobiol. A Chem.* **2014**, *294*, 96–109. [CrossRef]
114. Wang, F.; Yu, X.; Ge, M.; Wu, S. One-step synthesis of TiO_2/γ-Fe_2O_3/GO nanocomposites for visible light-driven degradation of ciprofloxacin. *Chem. Eng. J.* **2020**, *384*, 2–9. [CrossRef]
115. Liu, Z.; Ma, Z. Ag-SrTiO3/TiO_2 composite nanostructures with enhanced photocatalytic activity. *Mater. Res. Bull.* **2019**, *118*, 110492. [CrossRef]
116. Jahdi, M.; Mishra, S.B.; Nxumalo, E.N.; Mhlanga, S.D.; Mishra, A.K. Smart pathways for the photocatalytic degradation of sulfamethoxazole drug using F-Pd co-doped TiO_2 nanocomposites. *Appl. Catal. B Environ.* **2020**, *267*, 118716. [CrossRef]

117. Kowalska, K.; Maniakova, G.; Carotenuto, M.; Sacco, O.; Vaiano, V.; Lofrano, G.; Rizzo, L. Removal of carbamazepine, diclofenac and trimethoprim by solar driven advanced oxidation processes in a compound triangular collector based reactor: A comparison between homogeneous and heterogeneous processes. *Chemosphere* **2020**, *238*, 124665. [CrossRef]
118. Manasa, M.; Chandewar, P.R.; Mahalingam, H. Photocatalytic degradation of ciprofloxacin & norfloxacin and disinfection studies under solar light using boron & cerium doped TiO_2 catalysts synthesized by green EDTA-citrate method. *Catal. Today* **2020**, in press. [CrossRef]
119. Eskandarian, M.R.; Choi, H.; Fazli, M.; Rasoulifard, M.H. Effect of UV-LED wavelengths on direct photolytic and TiO_2 photocatalytic degradation of emerging contaminants in water. *Chem. Eng. J.* **2016**, *300*, 414–422. [CrossRef]
120. Lin, L.; Wang, H.; Jiang, W.; Mkaouar, A.R.; Xu, P. Comparison study on photocatalytic oxidation of pharmaceuticals by TiO_2-Fe and TiO_2-reduced graphene oxide nanocomposites immobilized on optical fibers. *J. Hazard. Mater.* **2017**, *333*, 162–168. [CrossRef]
121. Durán-Álvarez, J.C.; Avella, E.; Ramírez-Zamora, R.M.; Zanella, R. Photocatalytic degradation of ciprofloxacin using mono- (Au, Ag and Cu) and bi- (Au-Ag and Au-Cu) metallic nanoparticles supported on TiO_2 under UV-C and simulated sunlight. *Catal. Today* **2016**, *266*, 175–187. [CrossRef]
122. Sturini, M.; Speltini, A.; Maraschi, F.; Profumo, A.; Pretali, L.; Irastorza, E.A.; Fasani, E.; Albini, A. Photolytic and photocatalytic degradation of fluoroquinolones in untreated river water under natural sunlight. *Appl. Catal. B Environ.* **2012**, *119–120*, 32–39. [CrossRef]
123. Borowska, E.; Gomes, J.F.; Martins, R.C.; Quinta-Ferreira, R.M.; Horn, H.; Gmurek, M. Solar photocatalytic degradation of sulfamethoxazole by TiO_2 modified with noble metals. *Catalysts* **2019**, *9*, 500. [CrossRef]
124. Yu, S.; Wang, Y.; Sun, F.; Wang, R.; Zhou, Y. Novel mpg-C3N4/TiO_2 nanocomposite photocatalytic membrane reactor for sulfamethoxazole photodegradation. *Chem. Eng. J.* **2018**, *337*, 183–192. [CrossRef]
125. Sirtori, C.; Agüera, A.; Gernjak, W.; Malato, S. Effect of water-matrix composition on Trimethoprim solar photodegradation kinetics and pathways. *Water Res.* **2010**, *44*, 2735–2744. [CrossRef]
126. Samy, M.; Ibrahim, M.G.; Gar Alalm, M.; Fujii, M.; Ookawara, S.; Ohno, T. Photocatalytic degradation of trimethoprim using S-TiO_2 and Ru/WO3/ZrO_2 immobilized on reusable fixed plates. *J. Water Process Eng.* **2020**, *33*, 3–10. [CrossRef]
127. Calza, P.; Medana, C.; Carbone, F.; Giancotti, V.; Baiocchi, C. Characterization of intermediate compounds formed upon photoinduced degradation of quinolones by high-performance liquid chromatography/high-resolution multiple-stage mass spectrometry. *Rapid Commun. Mass Spectrom.* **2008**, *22*, 1533–1552. [CrossRef]
128. Hu, X.; Hu, X.; Peng, Q.; Zhou, L.; Tan, X.; Jiang, L.; Tang, C.; Wang, H.; Liu, S.; Wang, Y.; et al. Mechanisms underlying the photocatalytic degradation pathway of ciprofloxacin with heterogeneous TiO_2. *Chem. Eng. J.* **2020**, *380*, 122366. [CrossRef]
129. Zheng, X.; Xu, S.; Wang, Y.; Sun, X.; Gao, Y.; Gao, B. Enhanced degradation of ciprofloxacin by graphitized mesoporous carbon (GMC)-TiO_2 nanocomposite: Strong synergy of adsorption-photocatalysis and antibiotics degradation mechanism. *J. Colloid Interface Sci.* **2018**, *527*, 202–213. [CrossRef]
130. Gan, Y.; Wei, Y.; Xiong, J.; Cheng, G. Impact of post-processing modes of precursor on adsorption and photocatalytic capability of mesoporous TiO_2 nanocrystallite aggregates towards ciprofloxacin removal. *Chem. Eng. J.* **2018**, *349*, 1–16. [CrossRef]
131. Murgolo, S.; Yargeau, V.; Gerbasi, R.; Visentin, F.; El Habra, N.; Ricco, G.; Lacchetti, I.; Carere, M.; Curri, M.L.; Mascolo, G. A new supported TiO_2 film deposited on stainless steel for the photocatalytic degradation of contaminants of emerging concern. *Chem. Eng. J.* **2017**, *318*, 103–111. [CrossRef]
132. Silva, A.R.; Martins, P.M.; Teixeira, S.; Carabineiro, S.A.C.; Kuehn, K.; Cuniberti, G.; Alves, M.M.; Lanceros-Mendez, S.; Pereira, L. Ciprofloxacin wastewater treated by UVA photocatalysis: Contribution of irradiated TiO_2 and ZnO nanoparticles on the final toxicity as assessed by Vibrio fischeri. *RSC Adv.* **2016**, *6*, 95494–95503. [CrossRef]
133. Xing, X.; Du, Z.; Zhuang, J.; Wang, D. Removal of ciprofloxacin from water by nitrogen doped TiO_2 immobilized on glass spheres: Rapid screening of degradation products. *J. Photochem. Photobiol. A Chem.* **2018**, *359*, 23–32. [CrossRef]
134. Polliotto, V.; Pomilla, F.R.; Maurino, V.; Marcì, G.; Bianco Prevot, A.; Nisticò, R.; Magnacca, G.; Paganini, M.C.; Ponce Robles, L.; Perez, L.; et al. Different approaches for the solar photocatalytic removal of micro-contaminants from aqueous environment: Titania vs. hybrid magnetic iron oxides. *Catal. Today* **2019**, *328*, 164–171. [CrossRef]
135. Do, T.C.M.V.; Nguyen, D.Q.; Nguyen, K.T.; Le, P.H. TiO_2 and Au-TiO_2 nanomaterials for rapid photocatalytic degradation of antibiotic residues in aquaculture wastewater. *Materials* **2019**, *12*, 2434. [CrossRef]
136. Tsiampalis, A.; Frontistis, Z.; Binas, V.; Kiriakidis, G.; Mantzavinos, D. Degradation of sulfamethoxazole using iron-doped titania and simulated solar radiation. *Catalysts* **2019**, *9*, 612. [CrossRef]
137. Martini, J.; Orge, C.A.; Faria, J.L.; Pereira, M.F.R.; Soares, O.S.G.P. Catalytic advanced oxidation processes for sulfamethoxazole degradation. *Appl. Sci.* **2019**, *9*, 2652. [CrossRef]
138. Liang, R.; Van Leuwen, J.C.; Bragg, L.M.; Arlos, M.J.; Li Chun Fong, L.C.M.; Schneider, O.M.; Jaciw-Zurakowsky, I.; Fattahi, A.; Rathod, S.; Peng, P.; et al. Utilizing UV-LED pulse width modulation on TiO_2 advanced oxidation processes to enhance the decomposition efficiency of pharmaceutical micropollutants. *Chem. Eng. J.* **2019**, *361*, 439–449. [CrossRef]
139. Karaolia, P.; Michael-Kordatou, I.; Hapeshi, E.; Drosou, C.; Bertakis, Y.; Christofilos, D.; Armatas, G.S.; Sygellou, L.; Schwartz, T.; Xekoukoulotakis, N.P.; et al. Removal of antibiotics, antibiotic-resistant bacteria and their associated genes by graphene-based TiO_2 composite photocatalysts under solar radiation in urban wastewaters. *Appl. Catal. B Environ.* **2018**, *224*, 810–824. [CrossRef]

140. Arlos, M.J.; Hatat-Fraile, M.M.; Liang, R.; Bragg, L.M.; Zhou, N.Y.; Andrews, S.A.; Servos, M.R. Photocatalytic decomposition of organic micropollutants using immobilized TiO_2 having different isoelectric points. *Water Res.* **2016**, *101*, 351–361. [CrossRef] [PubMed]
141. Ramasundaram, S.; Seid, M.G.; Choe, J.W.; Kim, E.J.; Chung, Y.C.; Cho, K.; Lee, C.; Hong, S.W. Highly reusable TiO_2 nanoparticle photocatalyst by direct immobilization on steel mesh via PVDF coating, electrospraying, and thermal fixation. *Chem. Eng. J.* **2016**, *306*, 344–351. [CrossRef]
142. Murgolo, S.; Petronella, F.; Ciannarella, R.; Comparelli, R.; Agostiano, A.; Curri, M.L.; Mascolo, G. UV and solar-based photocatalytic degradation of organic pollutants by nano-sized TiO_2 grown on carbon nanotubes. *Catal. Today* **2015**, *240*, 114–124. [CrossRef]
143. Villanueva, M.E.; Puca, M.; Pérez Bravo, J.; Bafico, J.; Campo Dall Orto, V.; Copello, G.J. Dual adsorbent-photocatalytic keratin-TiO_2 nanocomposite for trimethoprim removal from wastewater. *New J. Chem.* **2020**, *44*, 10964–10972. [CrossRef]
144. Paredes, L.; Murgolo, S.; Dzinun, H.; Dzarfan Othman, M.H.; Ismail, A.F.; Carballa, M.; Mascolo, G. Application of immobilized TiO_2 on PVDF dual layer hollow fibre membrane to improve the photocatalytic removal of pharmaceuticals in different water matrices. *Appl. Catal. B Environ.* **2019**, *240*, 9–18. [CrossRef]
145. Li, C.; Zhu, N.; Dong, X.; Zhang, X.; Chen, T.; Zheng, S.; Sun, Z. Tuning and controlling photocatalytic performance of TiO_2/kaolinite composite towards ciprofloxacin: Role of 0D/2D structural assembly. *Adv. Powder Technol.* **2020**, *31*, 1241–1252. [CrossRef]
146. Suwannaruang, T.; Hildebrand, J.P.; Taffa, D.H.; Wark, M.; Kamonsuangkasem, K.; Chirawatkul, P.; Wantala, K. Visible light-induced degradation of antibiotic ciprofloxacin over Fe–N–TiO_2 mesoporous photocatalyst with anatase/rutile/brookite nanocrystal mixture. *J. Photochem. Photobiol. A Chem.* **2020**, *391*, 112371. [CrossRef]
147. Liu, Z.; Liu, X.; Lu, Q.; Wang, Q.; Ma, Z. $TiOF_2$/TiO_2 composite nanosheets: Effect of hydrothermal synthesis temperature on physicochemical properties and photocatalytic activity. *J. Taiwan Inst. Chem. Eng.* **2019**, *96*, 214–222. [CrossRef]
148. Liu, Z.; Tian, J.; Zeng, D.; Yu, C.; Huang, W.; Yang, K.; Liu, X.; Liu, H. Binary-phase TiO_2 modified Bi_2MoO_6 crystal for effective removal of antibiotics under visible light illumination. *Mater. Res. Bull.* **2019**, *112*, 336–345. [CrossRef]
149. Suwannaruang, T.; Kidkhunthod, P.; Chanlek, N.; Soontaranon, S.; Wantala, K. High anatase purity of nitrogen-doped TiO2 nanorice particles for the photocatalytic treatment activity of pharmaceutical wastewater. *Appl. Surf. Sci.* **2019**, *478*, 1–14. [CrossRef]
150. Feng, X.; Wang, P.; Hou, J.; Qian, J.; Ao, Y.; Wang, C. Significantly enhanced visible light photocatalytic efficiency of phosphorus doped TiO_2 with surface oxygen vacancies for ciprofloxacin degradation: Synergistic effect and intermediates analysis. *J. Hazard. Mater.* **2018**, *351*, 196–205. [CrossRef] [PubMed]
151. Li, C.; Sun, Z.; Zhang, W.; Yu, C.; Zheng, S. Highly efficient g-C_3N_4/TiO_2/kaolinite composite with novel three-dimensional structure and enhanced visible light responding ability towards ciprofloxacin and S. aureus. *Appl. Catal. B Environ.* **2018**, *220*, 272–282. [CrossRef]
152. Teixeira, S.; Mora, H.; Blasse, L.M.; Martins, P.M.; Carabineiro, S.A.C.; Lanceros-Méndez, S.; Kühn, K.; Cuniberti, G. Photocatalytic degradation of recalcitrant micropollutants by reusable Fe3O4/SiO_2/TiO_2 particles. *J. Photochem. Photobiol. A Chem.* **2017**, *345*, 27–35. [CrossRef]
153. Eckert, H.; Bobeth, M.; Teixeira, S.; Kühn, K.; Cuniberti, G. Modeling of photocatalytic degradation of organic components in water by nanoparticle suspension. *Chem. Eng. J.* **2015**, *261*, 67–75. [CrossRef]
154. Spanu, D.; Minguzzi, A.; Recchia, S.; Shahvardanfard, F.; Tomanec, O.; Zboril, R.; Schmuki, P.; Ghigna, P.; Altomare, M. An operando x-ray absorption spectroscopy study of a NiCu-TiO_2 photocatalyst for H2 evolution. *ACS Catal.* **2020**, *10*, 8293–8302. [CrossRef]
155. Majeed, I.; Nadeem, M.A.; Hussain, E.; Waterhouse, G.I.N.; Badshah, A.; Iqbal, A.; Nadeem, M.A.; Idriss, H. On the Synergism between Cu and Ni for Photocatalytic Hydrogen Production and their Potential as Substitutes of Noble Metals. *ChemCatChem* **2016**, *8*, 3146–3155. [CrossRef]
156. Lin, J.D.; Yan, S.; Huang, Q.D.; Fan, M.T.; Yuan, Y.Z.; Tan, T.T.Y.; Liao, D.W. TiO_2 promoted by two different non-noble metal cocatalysts for enhanced photocatalytic H2 evolution. *Appl. Surf. Sci.* **2014**, *309*, 188–193. [CrossRef]
157. Feng, S.; Zhao, J.; Bai, Y.; Liang, X.; Wang, T.; Wang, C. Facile synthesis of Mo-doped TiO_2 for selective photocatalytic CO_2 reduction to methane: Promoted H_2O dissociation by Mo doping. *J. CO2 Util.* **2020**, *38*, 1–9. [CrossRef]
158. Thakare, S.R.; Mate, V.R.; Urkude, K.; Gawande, S.B. Graphene-TiO_2-polyaniline nanocomposite: A new green and efficient catalyst as a alternative for noble metal and NaBH4 induced the reduction of 4-nitro phenol. *FlatChem* **2020**, *22*, 100179. [CrossRef]
159. Xiao, S.; Liu, P.; Zhu, W.; Li, G.; Zhang, D.; Li, H. Copper Nanowires: A Substitute for Noble Metals to Enhance Photocatalytic H2 Generation. *Nano Lett.* **2015**, *15*, 4853–4858. [CrossRef]